Unified asymptotic description of Gaussian pulse propagation of arbitrary initial pulse width in a Lorentz-type gain medium

Constantinos M. Balictsis*
10 Sokratous & Chiou Street, 15562 Cholargos, Attiki, Greece
(Received 22 May 2012; revised manuscript received 26 November 2012; published 16 January 2013)

An asymptotic approach is utilized in order to obtain a unified description of the propagated field dynamics due to an input Gaussian-modulated harmonic wave of arbitrary initial pulse width in a linear, causally dispersive gain medium, described by the single resonance Lorentz model. The asymptotic method of analysis is applied on the unified, exact integral representation of the propagated field, which is characterized by a unified complex phase function that depends upon the input field and gain medium parameters as well as upon the propagation distance in the medium. In order to apply the asymptotic method, an analysis of the evolution of the saddle point locations, which depend upon the dispersive properties of the gain medium, the temporal width, and the carrier frequency of the input Gaussian pulse as well as upon the propagation distance and of the topography of the real part of the unified phase function in the complex ω plane, must be performed. Upon the subsequent numerical application of the asymptotic method, the predictions of the unified asymptotic approach are found to be in exceptional agreement with the respective results of a purely numerical experiment for all considered initial pulse widths and lead to a unified model of Gaussian pulse propagation in a gain Lorentzian medium. According to this model, the propagated field is composed of pulse components, each being due to the asymptotic contribution of a respective relevant saddle point of the unified phase function. The instantaneous angular frequency of oscillation and the stationary point(s) of the envelope of each such pulse component are then obtained from the real and imaginary parts, respectively, of the corresponding relevant saddle point as it evolves in the complex ω plane. This theoretical approach may then yield particularly useful physical insights into attosecond pulse propagation.

DOI: 10.1103/PhysRevE.87.013304 PACS number(s): 02.70.−c, 42.25.Bs, 42.25.Fx

I. INTRODUCTION

A stream of research advances, most notably in the past decade, has enabled the reproducible generation, characterization, control, and shaping of ultrashort pulses of electromagnetic radiation and paved the way for a new research discipline, commonly referred to as attosecond science [1]. Its onset may be traced back to 2001 when the first attosecond light flashes were produced [2]. Successive developments in this discipline [3,4] led to the production of light flashes with duration less than 100 attoseconds (as) [5] using femtosecond laser technology capable of generating pulses in which the electric field performs a single oscillation [6]. Such developments enabled the real-time study of elementary particles and processes at an intra-atomic level which necessitate technologies with discriminatory capabilities at subfemtosecond time scales; in the offing are a host of important applications in physics, solid state physics, chemistry, biology, and medicine.

Recently, it became possible to synthesize wave forms of light pulses which consist of less than a full oscillation [7]. The advent of such pulses emphasizes the theoretical problem of providing an accurate description of their dynamical evolution as they propagate through and interact with a dispersive medium. Efforts to address this problem have concentrated on linear [8,9] as well as on nonlinear [10,11] media and systems. A number of these efforts [10–18] utilize the fundamental assumption concerning the slow variation of the pulse envelope in order to analytically describe the propagation characteristics of ultrashort and/or ultrawideband pulses; an unspecified degree of approximation is characteristic of the descriptions afforded by these efforts. An alternative means of investigating this pulse propagation problem is to use rigorously valid asymptotic approaches. The origin of such efforts may be traced back to the seminal work of Sommerfeld [19] and Brillouin [20] which resulted in the discovery of two, so-called, forerunners or precursors. More recently, Oughstun and his co-workers [8,9] resorted to modern asymptotic techniques in order to obtain a uniformly valid evaluation of the integral representation of the propagated field due to instantaneous rise and/or fall time or exponentially varying envelope input pulses in various linear, causally dispersive attenuative media and provided [21] a physical explanation of the resultant ultrashort pulse dynamics. Moreover, they concluded [22] that there exists a critical distance separating the complementary ranges of increased accuracy of approaches that are based upon either the slowly varying envelope approximation or that resort to asymptotic techniques. A variety of numerical techniques have also been employed in order to assess the accuracy of the predictions of ultrashort and/or ultrawideband pulse dynamics in temporally dispersive media and systems [23]. The first experimental verification of the asymptotic description appeared in 1969 [24] when the Sommerfeld and Brillouin precursors were observed at microwave frequencies, while more recently [25] they were observed in the optical domain.

Of particular importance in optics is the case of Gaussian pulse propagation in a dispersive medium. Garrett and McCumber [12] investigated this problem in a linear dispersive, absorbing or amplifying, medium. They showed that the propagating pulse remains very nearly Gaussian, with its peak amplitude traveling at the classical group velocity even when it is superluminal (i.e., greater than the vacuum speed of

*c.balictsis@biosolutions.gr

light) or negative and argued that this is due to the action of the dispersive medium on the early frequency components of the input Gaussian envelope. Crisp [13,14] investigated the propagation of small area coherent input pulses through a resonant medium. He showed that, as the propagation distance in an attenuative medium increases, the area of the propagating pulse decays exponentially to zero and its center of gravity moves with a velocity that may become superluminal. In an amplifying medium an input Gaussian pulse experiences significant asymmetric broadening and slows down. It was argued that the asymmetric energy absorption from, or radiation to, the pulse explains the superluminal values of the group velocity in an attenuative medium [12] as well as related experimental findings [26] in an amplifying medium. Chu and Wong [27] experimentally observed pulse propagation in a linear dispersive and absorptive medium at group velocities, even when they are superluminal, become infinite or even negative. Hoc *et al.* [28] have instead relied on approximations of the exact Wigner equation and asymptotic techniques in order to examine this propagation problem in a linear, homogeneous dispersive and absorptive medium. The investigations of Varoquaux *et al.* [16] regarding smoothly varying input pulses in a Lorentz medium showed that the propagating field may consist of two parts: the precursors and the main signal. They concluded that the propagating field due to an input Gaussian pulse does not contain any precursors and its peak travels with the classical group velocity. Christov [17] studied the propagation of an input pulse whose spectrum is significantly broader than the absorption band of a low density Lorentz medium and showed that the medium dispersion results in severe pulse distortion and the appearance of intensity oscillations. Vainshtein [15] reviewed the propagation of slowly varying envelope input pulses in linear, homogeneous, absorptive or amplifying, dispersive media. In particular, the dynamics of the main or principal part of the propagating field was examined from the ray point of view, the wave point of view, and the energy point of view. Tanaka *et al.* [29] utilized asymptotic techniques in order to investigate Gaussian wave propagation in an absorptive Lorentz medium. They examined the velocity of the wave packet and showed that it decreases in the absorption band in contrast to the group velocity which becomes infinite. They further argued that reported superluminal velocities [27] characterize the early part of the flight and are due to the distortion of the packet as it propagates in the anomalous dispersion region of the medium; subluminal velocities appear as the propagation distance increases. Finally, Balictsis and Oughstun [30–33] resorted to modern asymptotic methods [9,34–36] in order to provide a complete description of the propagated field due to an input Gaussian-modulated harmonic wave in a linear, causally dispersive, and absorptive Lorentz medium. This asymptotic description is uniformly valid for all initial pulse widths and reduces to the opposite limiting descriptions that are valid either in the ultrashort pulse regime or in the slowly varying envelope pulse regime; it was completely verified upon comparison with two different, numerical experiments [9,37,38]. These results were finally shown to be a special case of a new, model of Gaussian pulse propagation in a linear, causally dispersive, and absorptive Lorentz-type medium.

Recently, Safian *et al.* [39] utilized the classical steepest descent approach [9,20] in order to describe the propagated field in a linear, causally dispersive, active Lorentzian medium, ignoring saturation and related nonlinear effects. Their theoretical and numerical investigations of an input unit-step function modulated harmonic field showed that the Sommerfeld precursor does not appear in active media, while the transient and the main parts of the propagating field are almost indistinguishable. Their cursory, and strictly numerical, consideration of an input Gaussian-modulated harmonic signal resulted in superluminal velocities for the propagated field envelope. Superluminal propagation of Gaussian input pulses, in a linear inverted two-level atomic medium, has been theoretically considered by Chiao [18] and was observed experimentally [40,41]. The intriguing problem in dispersive wave theory concerning the propagation velocities of light continues to attract significant research interest [8,9].

Here, a modern asymptotic method of analysis [9,34] is applied in order to obtain a unified description of the propagated field due to an input Gaussian-modulated harmonic signal of arbitrary initial pulse width in a linear, causally dispersive gain Lorentzian medium. In particular, the classical [39], as well as the unified, exact integral formulations of the canonical problem of interest are described in the next section. The following section presents the unified model of Gaussian pulse propagation in a gain Lorentzian medium, which results from the unified asymptotic approach. The next section compares the results of the unified asymptotic analysis with the corresponding results of both the classical asymptotic approach as well as the numerical experiment, completely verifying this model of Gaussian pulse propagation in a gain Lorentzian medium, and provides a discussion of the observed propagated field dynamics. The final section provides the conclusions of the research reported here. Appendix A is a study of the dynamical evolution of the saddle points of the unified phase function, while Appendix B presents the mathematical proof of the unified model of Gaussian pulse propagation in a gain Lorentzian medium, and, finally, Appendix C presents an analysis of the real part of the unified phase function along the real frequency axis which is then utilized in order to obtain an approximate, heuristic evaluation of the propagated field. In the ensuing, nonlinear and saturation effects in gain media are considered to be negligible.

II. FORMULATION OF THE CANONICAL PROBLEM

A. Classical, exact integral formulation of Gaussian pulse propagation in a linear, causally dispersive medium

The propagated field due to an input, Gaussian-modulated harmonic wave in the positive z direction of a linear, homogeneous, isotropic, temporally dispersive, nonhysteretic medium filling the semi-infinite space $z \geqslant 0$ (where there are no charge or current sources) is given exactly by the integral representation [9,30–33,39]

$$A(z,t) = \frac{1}{2\pi}\mathrm{Re}\left\{ i \int_{-\infty}^{+\infty} \tilde{U}(\omega-\omega_c)\exp\left[\frac{z}{c}\phi(\omega,\theta')\right] d\omega \right\} \tag{1}$$

for all $z \geqslant 0$, where the scalar function $A(z,t)$ may represent either the scalar potential, or the amplitude of any orthogonal component of the electric field, magnetic field, Hertz vector, or vector potential (henceforth, the notation Re{·} represents the real part, while the notation Im{·} represents the imaginary part of the quantity inside the curly brackets).

Here, the complex spectral amplitude function

$$\begin{aligned}\tilde{U}(\omega-\omega_c) &= \exp[-i(\omega t_0+\psi)]\tilde{u}(\omega-\omega_c)\\ &= \exp(-i\psi)\left\{\sqrt{\pi}T\exp(-i\omega_c t_0)\right.\\ &\quad\left.\times\exp\left[-\frac{T^2(\omega-\omega_c)^2}{4}\right]\right\} \qquad (2)\end{aligned}$$

has been introduced, where $\tilde{u}(\omega)$,

$$\begin{aligned}\tilde{u}(\omega) &= \int_{-\infty}^{+\infty} u(t)e^{i\omega t}dt = \int_{-\infty}^{+\infty}\exp\left[-\left(\frac{t-t_0}{T}\right)^2\right]e^{i\omega t}dt\\ &= \sqrt{\pi}T\exp\left(-\frac{T^2\omega^2}{4}\right)\exp(i\omega t_0), \qquad (3)\end{aligned}$$

denotes the temporal spectrum of the input Gaussian envelope which is centered around the instant $t_0 > 0$, with a full width given by $2T$, while ω_c denotes the constant applied carrier frequency and the constant phase term ψ is chosen to be $\pi/2$ for a cosine wave or zero for a sine wave.

The complex phase function appearing in Eq. (1) is given by

$$\phi(\omega,\theta') = i\frac{c}{z}[\tilde{k}(\omega)z-\omega(t-t_0)] = i\omega[n(\omega)-\theta'], \qquad (4)$$

where

$$\theta' = \theta - \frac{ct_0}{z} = \frac{c}{z}(t-t_0) \qquad (5)$$

is an appropriate, nondimensional, space-time parameter. In Eq. (4), $\tilde{k}(\omega) = [\omega n(\omega)]/c$ is the complex wave number, $n(\omega) = \sqrt{\varepsilon(\omega)}$ is the complex index of refraction of the dispersive medium whose relative magnetic permeability is $\mu = 1$ and whose relative complex dielectric permittivity is given by $\varepsilon(\omega)$, and where c is the vacuum speed of light.

Equation (1) constitutes the classical, exact integral expression of the propagated field. Moreover, the function $\tilde{U}(\omega-\omega_c)$, defined in Eq. (2), is the classical spectral amplitude function, while the function $\phi(\omega,\theta')$, which is defined in Eq. (4), is the classical phase function. The input Gaussian envelope is considered to extend over all time, and in order for the integral appearing in Eq. (3) to converge at $t = \pm\infty$, the original contour of integration C may be taken to be the real frequency axis, as shown in Eq. (1). Any other contour in the complex ω plane that is homotopic to the real frequency axis can also be used in Eq. (1) as a valid integration path [42]. Although the spectral function $\tilde{u}(\omega)$, given in Eq. (3), represents the Fourier spectrum of the input Gaussian envelope, it may also be regarded as being the Laplace transform of the same envelope to an excellent

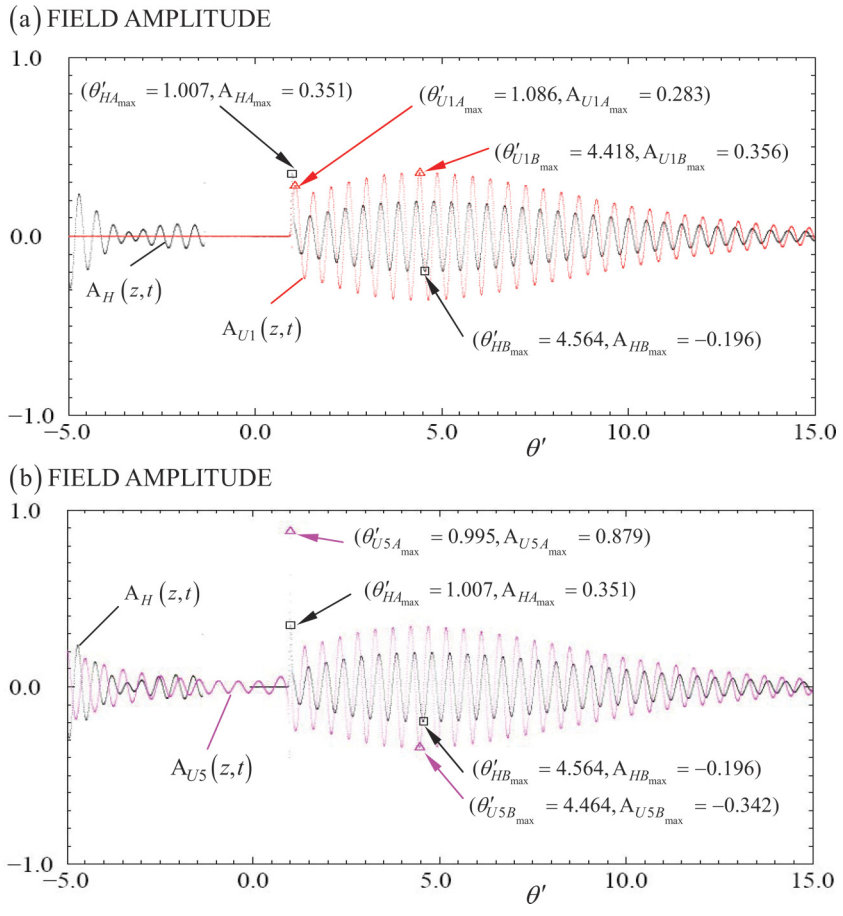

FIG. 1. (Color online) The dynamical field evolution due to an input unit-amplitude Gaussian-modulated harmonic (sine) wave with initial pulse width $2T = 0.2$ fs and carrier frequency $\omega_c = 1.0 \times 10^{15}$ s^{-1}, at a propagation distance $z = 1.0\ \mu$m in a single resonance Lorentz-type dispersive and gain medium. In both diagrams, the solid line (online denoted in black) represents the field amplitude $A_H(z,t)$ evaluated using the Hosono code. Moreover, the squares (online denoted in black) denote (absolute) field amplitude maxima. In (a) the solid line (online denoted in red) represents the amplitude of the pulse component $A_{U1}(z,t)$ due to the asymptotic contribution of the saddle point SP_{U1} evaluated using the unified asymptotic theory. The triangles (online denoted in red) denote the respective (absolute) pulse amplitude maxima. In (b) the solid line (online denoted in magenta) represents the amplitude of the pulse component $A_{U5}(z,t)$ due to the asymptotic contribution of the saddle point SP_{U5} evaluated using the unified asymptotic theory. The triangles (online denoted in magenta) denote the respective (absolute) pulse amplitude maxima.

degree of approximation provided that one chooses $t_0 > 0$ to be sufficiently larger than the initial pulse width $2T$. The time behavior of the input Gaussian envelope is then exponentially small for all $t < 0$.

B. Unified, exact integral formulation of Gaussian pulse propagation in a linear, causally dispersive medium

In order to obtain an asymptotic approximation of the propagated field which is uniformly valid not only in the space-time parameter θ' but also in the input pulse and dispersive medium parameters, the classical integral formulation of Gaussian pulse propagation is rewritten as

$$A(z,t) = \frac{1}{2\pi}\mathrm{Re}\left\{ i \int_C \tilde{U}_U \exp\left[\frac{z}{c}\Phi_U(\omega,\theta')\right] d\omega \right\} \qquad (6)$$

for all $z \geqslant 0$, where the complex spectral amplitude $\tilde{U}_U$ is independent of ω and is given by

$$\tilde{U}_U = \sqrt{\pi} T \exp[-i(\omega_c t_0 + \psi)], \qquad (7)$$

and where the complex phase function $\Phi_U(\omega,\theta')$ also appearing here is given by

$$\Phi_U(\omega,\theta') = \phi(\omega,\theta') - \frac{cT^2}{4z}(\omega - \omega_c)^2; \qquad (8)$$

in Eq. (8), $\phi(\omega,\theta')$ is the classical phase function given by Eq. (4) and $n(\omega)$ is the refractive index of the dispersive medium. In Eqs. (6) and (8) the dimensionless, real space-time parameter θ' is the same as given by Eq. (5). The contour of integration C appearing in Eq. (6) may be taken to be either the real frequency axis, as is the case in the classical integral representation of the propagated field, or any other contour in the complex ω plane that is homotopic to the real frequency axis.

Henceforth, Eq. (6) constitutes the unified, exact integral expression of the propagated field; an analogous expression forms the basis for the asymptotic analysis of Gaussian pulse propagation in an absorptive dielectric medium [9,31–33]. The frequency independent spectral amplitude $\tilde{U}_U$, which is defined in Eq. (7), is the unified spectral amplitude, and the phase function $\Phi_U(\omega,\theta')$, which is defined in Eq. (8), is the unified phase function. It is evident from Eq. (8) that the unified phase function depends not only upon the dispersive properties of the medium, as displayed by the first term on the right-hand side, but also upon the temporal width $2T$ and carrier frequency ω_c of the input Gaussian pulse as well as upon the propagation distance z in the dispersive medium, as displayed by the second term on the right-hand side. When the unified integral formulation of Gaussian pulse propagation is used as the starting point in the asymptotic analysis, the obtained unified asymptotic description of the propagated field will reduce to the respective classical asymptotic description in the limit as the initial pulse width approaches zero from above and/or as the propagation distance in the dispersive medium tends to infinity; in general it will be different from the classical asymptotic

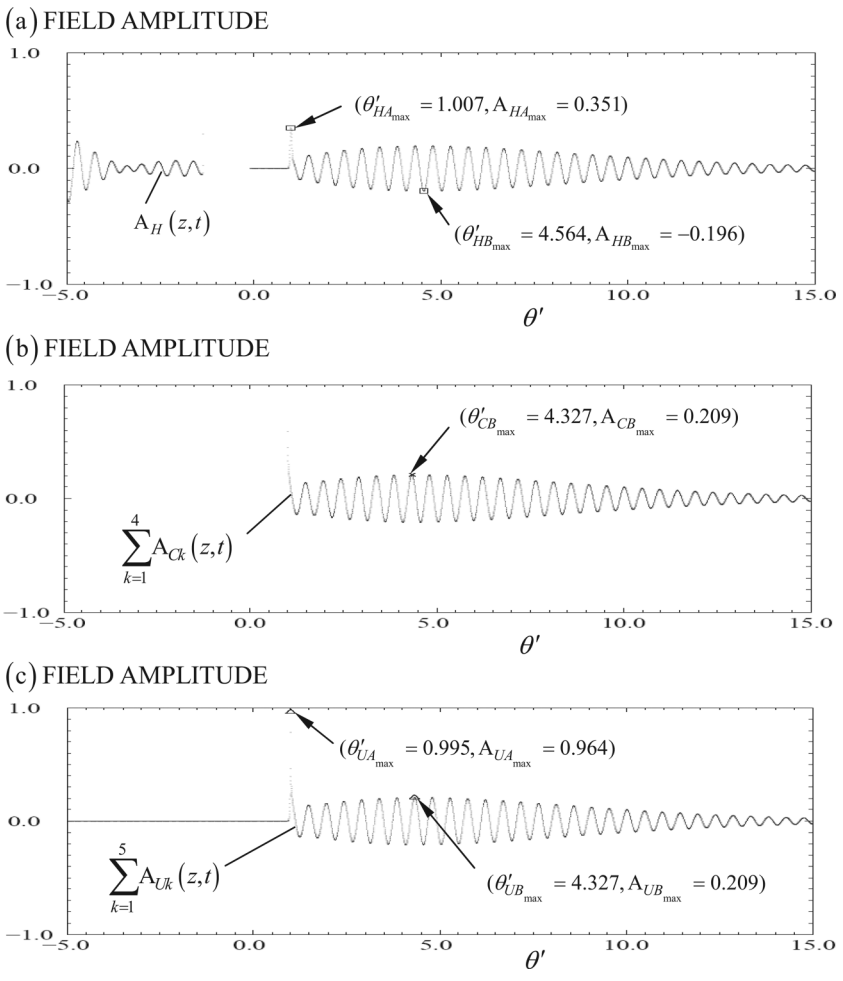

FIG. 2. The dynamical evolution of the propagated field evaluated using (a) the Hosono code $[A_H(z,t)]$, (b) the classical nonuniform asymptotic theory $[\sum_{k=1}^{4} A_{Ck}(z,t)]$, and (c) the unified asymptotic theory $[\sum_{k=1}^{5} A_{Uk}(z,t)]$, due to an input unit-amplitude Gaussian-modulated harmonic (sine) wave with initial pulse width $2T = 0.2$ fs and carrier frequency $\omega_c = 1.0 \times 10^{15}$ s^{-1}, at a propagation distance $z = 1.0$ μm in a single resonance Lorentz-type dispersive and gain medium. The squares in the top diagram, the cross in the middle diagram, and the triangles in the bottom diagram denote (absolute) field amplitude maxima. In the middle diagram the (total) field amplitude is due to the (algebraic sum of the) asymptotic contributions of the relevant saddle points SP_{Ck}, $k = 1,2,\ldots,4$, of the classical phase function. In the bottom diagram the (total) field amplitude is due to the (algebraic sum of the) asymptotic contributions of the relevant saddle points SP_{Uk}, $k = 1,5$, of the unified phase function.

description. Indeed, the implementation of each asymptotic approach is critically dependent upon the phase function appearing in the corresponding integral representation of the propagated field, and when $2T$ approaches zero from above and/or when z tends to infinity, $\Phi_U(\omega,\theta')$ reduces to $\phi(\omega,\theta')$. Notice also that in the limit as $2T$ approaches zero from above, $\tilde{U}(\omega-\omega_c)$ reduces to $\tilde{U}_U$.

C. Single resonance Lorentz-type dispersive and gain medium

The problem considered here refers to the case of a gain medium occupying the half space $z \geqslant 0$. In particular, a single resonance Lorentz-type dielectric model with negative oscillator strength is chosen to represent an inverted two-level atomic medium. Ignoring the effect of inhomogeneous line broadening, the index of refraction is given by [18,39]

$$n(\omega) = \left(1 + \frac{b^2}{\omega^2 - \omega_0^2 + i2\delta\omega}\right)^{1/2}, \tag{9}$$

where ω_0 is the resonance frequency depicting the frequency difference between the two atomic levels, b^2 is the square of the plasma frequency of this medium, and δ is the resonance linewidth. Hereafter, use is made of the medium parameter values utilized in Ref. [39], viz., $\omega_0 = 4.0 \times 10^{15}\ \mathrm{s}^{-1}$, $b^2 = 1.0 \times 10^{30}\ \mathrm{s}^{-2}$, and $\delta = 0.2 \times 10^{15}\ \mathrm{s}^{-1}$. The Lorentz-type active model is a causal model [43], with the index of refraction in Eq. (9) satisfying the Kramers-Krönig relations [39].

For the chosen gain medium, $n(\omega)$ is a holomorphic function in the entire complex ω plane except at the two (inner) branch points $\omega'_{\pm} = \pm[\omega_1^2 - \delta^2]^{1/2} - i\delta$ where $n(\omega)$ vanishes, and also at the two (outer) branch points $\omega_{\pm} = \pm[\omega_0^2 - \delta^2]^{1/2} - i\delta$ where $n(\omega)$ becomes infinite, with $\omega_1^2 = \omega_0^2 - b^2$. The line segments $\omega_-\omega'_-$ and $\omega'_+\omega_+$ are, respectively, the left and right branch cuts of $n(\omega)$.

III. THE UNIFIED MODEL OF GAUSSIAN PULSE PROPAGATION IN A LORENTZ-TYPE DISPERSIVE AND GAIN MEDIUM

The methodology that must be followed in order to obtain an analytic evaluation of the unified integral formulation of Gaussian pulse propagation in a gain Lorentzian medium, utilizing modern asymptotic methods, constitutes the unified asymptotic approach and essentially follows the general procedure utilized in the case of a dispersive and absorptive dielectric medium [9,31–33].

For fixed, but otherwise arbitrary, values of the initial pulse width $2T$ and carrier frequency ω_c of the input Gaussian-modulated harmonic wave, and at a sufficiently large, but otherwise arbitrary, fixed propagation distance z in a single resonance Lorentz-type gain medium, the unified phase

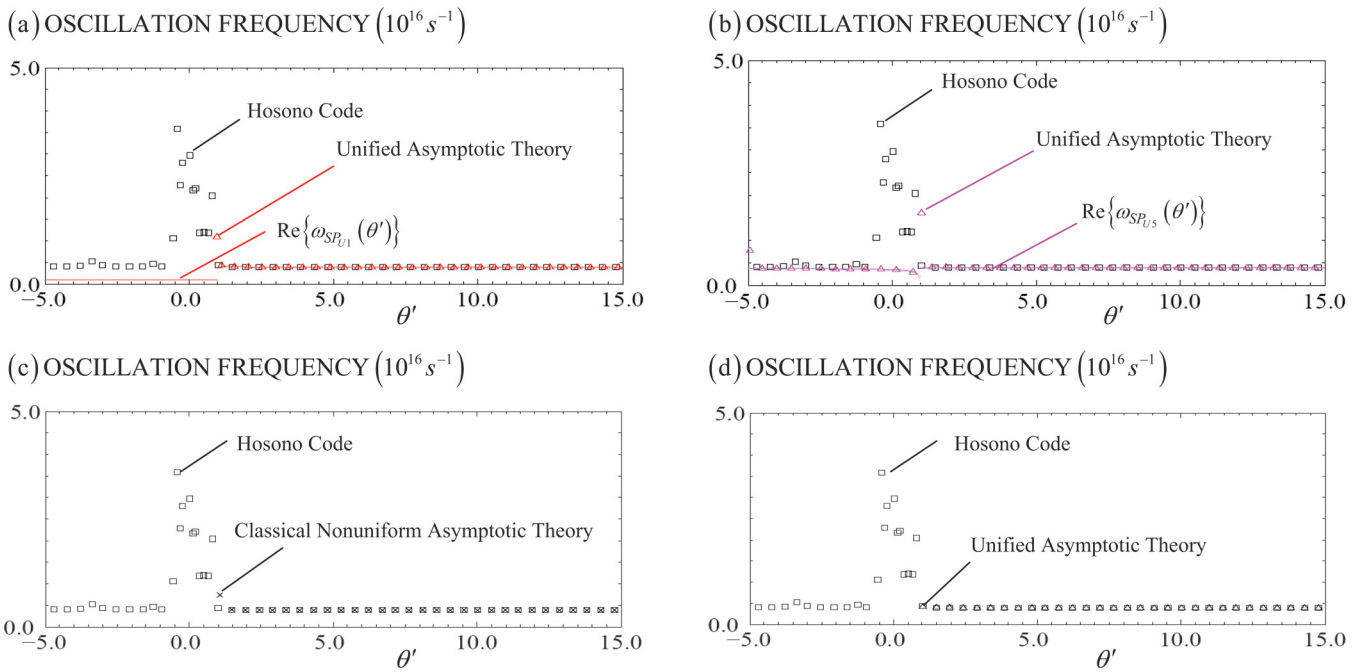

FIG. 3. (Color online) The instantaneous angular frequency of oscillation of the propagated field due to an input unit-amplitude Gaussian-modulated harmonic (sine) wave with initial pulse width $2T = 0.2$ fs and carrier frequency $\omega_c = 1.0 \times 10^{15}\ \mathrm{s}^{-1}$, at a propagation distance $z = 1.0\ \mu$m in a single resonance Lorentz-type dispersive and gain medium. In all diagrams, the squares (online denoted in black) denote the Hosono code evaluated oscillation frequency. In (a) the triangles (online denoted in red) denote the unified asymptotic theory evaluated oscillation frequency and is due to the asymptotic contribution of the saddle point SP_{U1}. Moreover, the solid line (online denoted in red) represents the real part of the respective saddle point SP_{U1}. In (b) the triangles (online denoted in magenta) denote the unified asymptotic theory evaluated oscillation frequency and is due to the asymptotic contribution of the saddle point SP_{U5}. Moreover, the solid line (online denoted in magenta) represents the real part of the respective saddle point SP_{U5}. In (c) the crosses (online denoted in black) denote the instantaneous frequency of oscillation evaluated from the classical nonuniform asymptotic theory. In (d) the triangles (online denoted in black) denote the instantaneous frequency of oscillation evaluated from the unified asymptotic theory.

$\Phi_U(\omega,\theta')$ is a function not only of the complex frequency ω but also of the real space-time parameter θ'. Therefore, the unified asymptotic approach begins with a determination of the evolution of the saddle points of $\Phi_U(\omega,\theta')$ as a function of θ', in the complex ω plane. According to the study of the saddle point dynamics in Appendix A, for the considered single resonance Lorentz gain medium, $\Phi_U(\omega,\theta')$ has five saddle points, SP_{Uk}, $k = 1,2,\ldots,5$, which are isolated and of first order for all values of θ', irrespective of the characteristics of the input Gaussian pulse and the distance of propagation in this dispersive medium [henceforth, the term $\omega_{SP_{Uk}}(\theta')$ will also be used to interchangeably denote the location of the saddle point SP_{Uk} of $\Phi_U(\omega,\theta')$ as it evolves with θ' in the complex ω plane]. Subsequently, an evaluation of the real part of the unified phase function $X_U(\omega,\theta')$ at each of the saddle points determines their relative dominance (i.e., the level of exponential decay associated with each one of them) for each value of θ'. This is then followed by an examination of the isotimic contours of $X_U(\omega,\theta')$ in order to deduce for each of the saddle points of $\Phi_U(\omega,\theta')$ the regions in the complex ω plane where $X_U(\omega,\theta')$ attains values that are less than its value at the respective saddle point, for a given value of θ'. The knowledge acquired in the preceding steps concerning the dynamics of the saddle points SP_{Uk}, $k = 1,2,\ldots,5$, of $\Phi_U(\omega,\theta')$ is a prerequisite in order to proceed with the remaining steps in the unified asymptotic approach. In particular, the next step is to apply Cauchy's residue theorem [42] in order to deform the original integration path C appearing in the unified, exact integral expression (6) of the propagated field into a new path $P(\theta')$ which passes through all relevant saddle points of $\Phi_U(\omega,\theta')$ for a given value of θ'. As θ' varies continuously in its domain $\theta' \in (-\infty, +\infty)$, the deformed path $P(\theta')$ is required to move continuously in the complex ω plane so as to pass through all the relevant saddle points of $\Phi_U(\omega,\theta')$ for any given value of θ' in such a manner that it may be divisible into a superposition of paths $P_{Ul}(\theta')$, each being an Olver-type path with respect to a single relevant saddle point SP_{Ul} which it must only cross. Since the constant unified spectral amplitude $\tilde{U}_U$ is holomorphic everywhere in the complex ω plane, this step in the unified asymptotic approach allows the original contour integral $A(z,t)$, which is taken along C, to be written as a superposition of deformed contour integrals $I_{Ul}(z,\theta')$, each of which has the same integrand as $A(z,t)$ but is taken along the respective component path $P_{Ul}(\theta')$ of $P(\theta')$, in the form

$$A(z,t) = \sum_l I_{Ul}(z,\theta') = \sum_l \left(\frac{1}{2\pi} \mathrm{Re}\left\{ i \int_{P_{Ul}(\theta')} \tilde{U}_U \exp\left[\frac{z}{c} \Phi_U(\omega,\theta') \right] d\omega \right\} \right), \tag{10}$$

for any given value of θ'. The final, crucial step in the unified asymptotic approach for Gaussian pulse propagation of arbitrary initial pulse width is to apply Olver's asymptotic method [34] to each of the deformed contour integrals $I_{Ul}(z,\theta')$ appearing in Eq. (10), which yields an asymptotic description

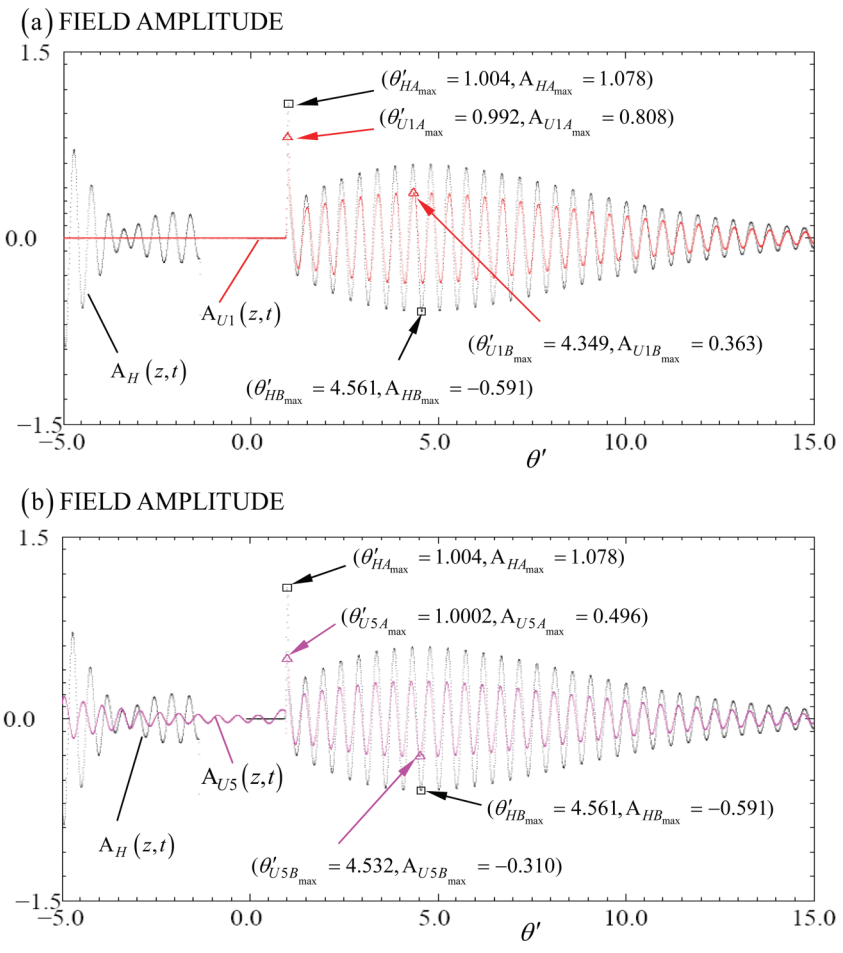

FIG. 4. (Color online) The dynamical field evolution due to an input unit-amplitude Gaussian-modulated harmonic (sine) wave with initial pulse width $2T = 0.2$ fs and carrier frequency $\omega_c = 4.0 \times 10^{15}$ s^{-1}, at a propagation distance $z = 1.0\,\mu$m in a single resonance Lorentz-type dispersive and gain medium. In both diagrams, the solid line (online denoted in black) represents the field amplitude $A_H(z,t)$ evaluated using the Hosono code. Moreover, the squares (online denoted in black) denote (absolute) field amplitude maxima. In (a) the solid line (online denoted in red) represents the amplitude of the pulse component $A_{U1}(z,t)$ due to the asymptotic contribution of the saddle point SP_{U1} evaluated using the unified asymptotic theory. The triangles (online denoted in red) denote the respective (absolute) pulse amplitude maxima. In (b) the solid line (online denoted in magenta) represents the amplitude of the pulse component $A_{U5}(z,t)$ due to the asymptotic contribution of the saddle point SP_{U5} evaluated using the unified asymptotic theory. The triangles (online denoted in magenta) denote the respective (absolute) pulse amplitude maxima.

of the propagated field that is uniformly valid for all θ' and is given by the general expression

$$A(z,t) = \sum_l A_{Ul}(z,t) = \sum_l \left(\frac{1}{2\pi} \mathrm{Re} \left\{ i2 \exp\left[\frac{z}{c} \Phi_U\left(\omega_{SP_{Ul}}, \theta'\right) \right] \left(\frac{\pi c}{z} \right)^{1/2} \times \frac{\tilde{U}_U}{2\left[-\frac{1}{2!} \frac{d^2 \Phi_U(\omega_{SP_{Ul}}, \theta')}{d\omega^2} \right]^{1/2}} \left[1 + O\left(\frac{1}{z} \right) \right] \right\} \right) \quad (11)$$

for sufficiently large values of the propagation distance z in the considered single resonance Lorentz gain medium. Notice that in Eqs. (10) and (11) the summation over l extends only over those saddle points SP_{Ul} of $\Phi_U(\omega,\theta')$ that are relevant at the particular value of θ' considered. Each term $A_{Ul}(z,t)$, which results from the application of Olver's method to the respective term $I_{Ul}(z,\theta')$ in Eq. (10), is then given by

$$A_{Ul}(z,t) = \frac{1}{2\pi} \mathrm{Re} \left\{ i2 \exp\left[\frac{z}{c} \Phi_U\left(\omega_{SP_{Ul}}, \theta'\right) \right] \left(\frac{\pi c}{z} \right)^{1/2} \times \frac{\tilde{U}_U}{2\left[-\frac{1}{2!} \frac{d^2 \Phi_U(\omega_{SP_{Ul}}, \theta')}{d\omega^2} \right]^{1/2}} \left[1 + O\left(\frac{1}{z} \right) \right] \right\}. \quad (12)$$

Since the dynamics of the saddle points of $\Phi_U(\omega,\theta')$ depend not only upon the medium parameters but also upon the input field parameters and the propagation distance in the dispersive medium, the unified asymptotic approach must be performed each time one of these parameters changes value.

This unified asymptotic approach is shown in Appendix B to lead to a unified model of Gaussian pulse propagation in a gain Lorentzian medium, which states that the dynamical evolution of the propagated field $A(z,t)$ due to an input Gaussian-modulated harmonic wave of arbitrary initial pulse width $2T$ at a fixed, but otherwise arbitrary, propagation distance z in a linear, causally dispersive gain medium described by the single resonance Lorentz model expression (9) is given by

$$A(z,t) = \sum_{l=1}^{m} A_{Ul}(z,t), \quad m \leqslant 5, \quad (13)$$

and is composed of the pulse components $A_{Ul}(z,t)$ given in Eq. (12), each of which is due to the asymptotic contribution of a respective relevant saddle point $\omega_{SP_{Ul}}(\theta')$ of the unified phase function $\Phi_U(\omega,\theta')$ appearing in the unified, exact integral expression (9) for $A(z,t)$. The propagation characteristics of each such pulse component of the propagated field may be obtained from the dynamics of the respective relevant saddle point. In particular:

(I) The evolution with time of the instantaneous angular frequency of oscillation $\omega_{IFO_{Ul}}(\theta')$ of $A_{Ul}(z,t)$ is given by Eq. (B12), viz., $\omega_{IFO_{Ul}}(\theta') = \mathrm{Re}\{\omega_{SP_{Ul}}(\theta')\} + \Delta_{1_{Ul}}(\theta')$, where $\Delta_{1_{Ul}}(\theta')$ is given by Eqs. (B9)–(B11). Therefore, $\omega_{IFO_{Ul}}(\theta')$ is

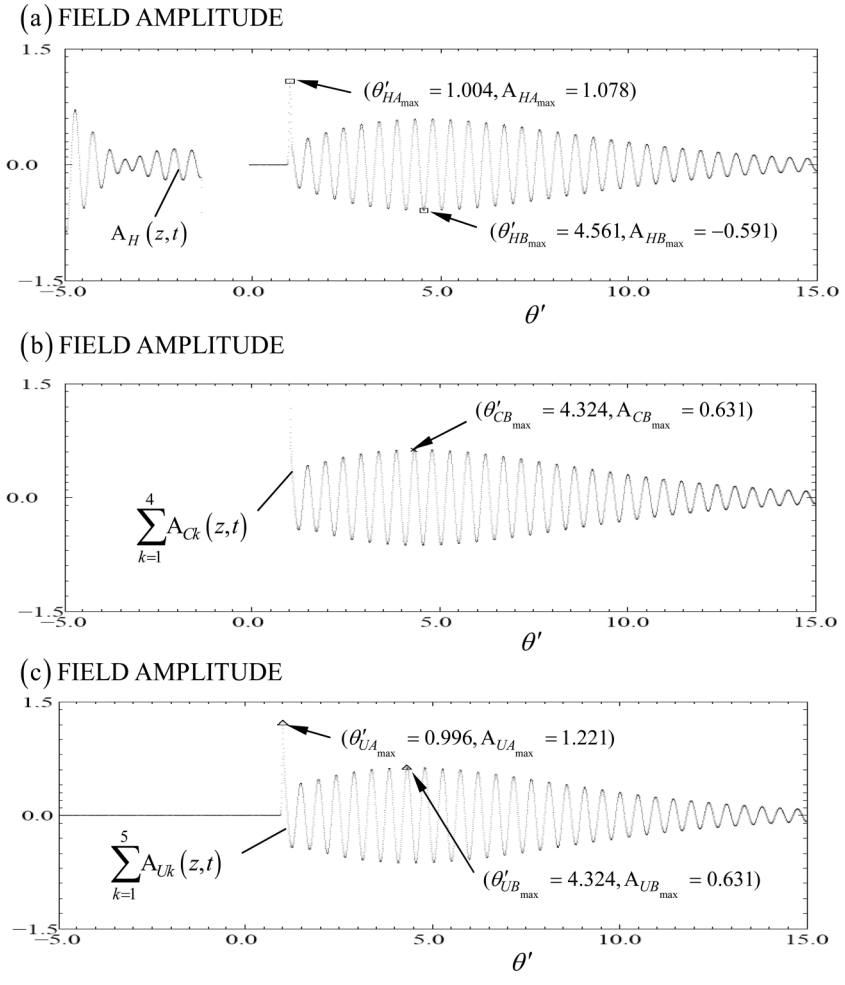

FIG. 5. The dynamical evolution of the propagated field evaluated using (a) the Hosono code $[A_H(z,t)]$, (b) the classical nonuniform asymptotic theory $[\sum_{k=1}^{4} A_{Ck}(z,t)]$, and (c) the unified asymptotic theory $[\sum_{k=1}^{5} A_{Uk}(z,t)]$, due to an input unit-amplitude Gaussian-modulated harmonic (sine) wave with initial pulse width $2T = 0.2$ fs and carrier frequency $\omega_c = 4.0 \times 10^{15}$ s^{-1}, at a propagation distance $z = 1.0$ μm in a single resonance Lorentz-type dispersive and gain medium. The squares in the top diagram, the cross in the middle diagram, and the triangles in the bottom diagram denote (absolute) field amplitude maxima. In the middle diagram the (total) field amplitude is due to the (algebraic sum of the) asymptotic contributions of the relevant saddle points SP_{Ck}, $k = 1,2,\ldots,4$, of the classical phase function. In the bottom diagram the (total) field amplitude is due to the (algebraic sum of the) asymptotic contributions of the relevant saddle points SP_{Uk}, $k = 1,5$, of the unified phase function.

given by the real part of the respective relevant saddle point location $\mathrm{Re}\{\omega_{SP_{UI}}(\theta')\}$ as it evolves in the complex ω plane, when the term $\Delta_{1_{UI}}(\theta')$ becomes (asymptotically) negligible.

(II) The envelope of $A_{UI}(z,t)$ exhibits its stationary point(s) when the relation in Eq. (B21) is satisfied, viz., $\mathrm{Im}\{\omega_{SP_{UI}}(\theta')\} = \Delta_{2_{UI}}(\theta')$, where $\Delta_{2_{UI}}(\theta')$ is given by Eqs. (B15)–(B17). The stationary point(s) of the envelope of $A_{UI}(z,t)$ may occur when the trajectory followed by the respective relevant saddle point $\omega_{SP_{UI}}(\theta')$ intersects the real frequency axis in the complex ω plane, when the term $\Delta_{2_{UI}}(\theta')$ becomes (asymptotically) negligible.

(III) If the trajectory followed in the complex ω plane by the relevant saddle point $\omega_{SP_{UI}}(\theta')$ intersects the real frequency axis, this occurs at the location of a stationary point of the real part of the unified phase function along this axis [i.e., at the location of a local maximum or minimum of the function $X_U(\omega_r)$].

IV. DISCUSSION

In order to demonstrate the accuracy and range of validity of the unified asymptotic approach compared to the classical asymptotic approach, Figs. 1–11 illustrate the dynamical evolution of the pulse component(s), the respective (total) propagated field and their corresponding instantaneous frequencies of oscillation pertaining to four different cases characterized by a different set for the input Gaussian-modulated sine field parameters, and the propagation distance in the single resonance Lorentz-type gain medium. Figures 1–3 constitute the first case, where the initial pulse width $2T = 0.2$ fs, the applied carrier frequency $\omega_c = 1.0 \times 10^{15}$ s^{-1}, and the propagation distance $z = 1.0$ μm correspond to an input ultrashort Gaussian pulse with carrier frequency below the amplification band of the gain medium, such that the sine wave at the input plane $z = 0$ approximately completes only 0.032 oscillations under the full width at the e^{-1} maximum points of the input Gaussian envelope. In Figs. 4–6, which constitute the second case, the applied carrier frequency has increased to $\omega_c = 4.0 \times 10^{15}$ s^{-1}, which lies near the center of the medium's amplification band, while the initial pulse width and the propagation distance remain the same as those utilized in the first case; here, the sine wave at the input plane approximately completes only 0.127 oscillations. In the third case, depicted in Figs. 7 and 8, the initial pulse width is broadened to $2T = 20.0$ fs while the applied carrier frequency and the propagation distance are those utilized in the first case; here, the sine wave at the input plane approximately completes 3.183 oscillations. Finally, in the fourth case, depicted in Figs. 9–11, the propagation distance is shortened to $z = 0.75$ μm while the remaining input Gaussian-modulated sine field parameters remain the same as those utilized in the first case; the sine wave at the input plane approximately

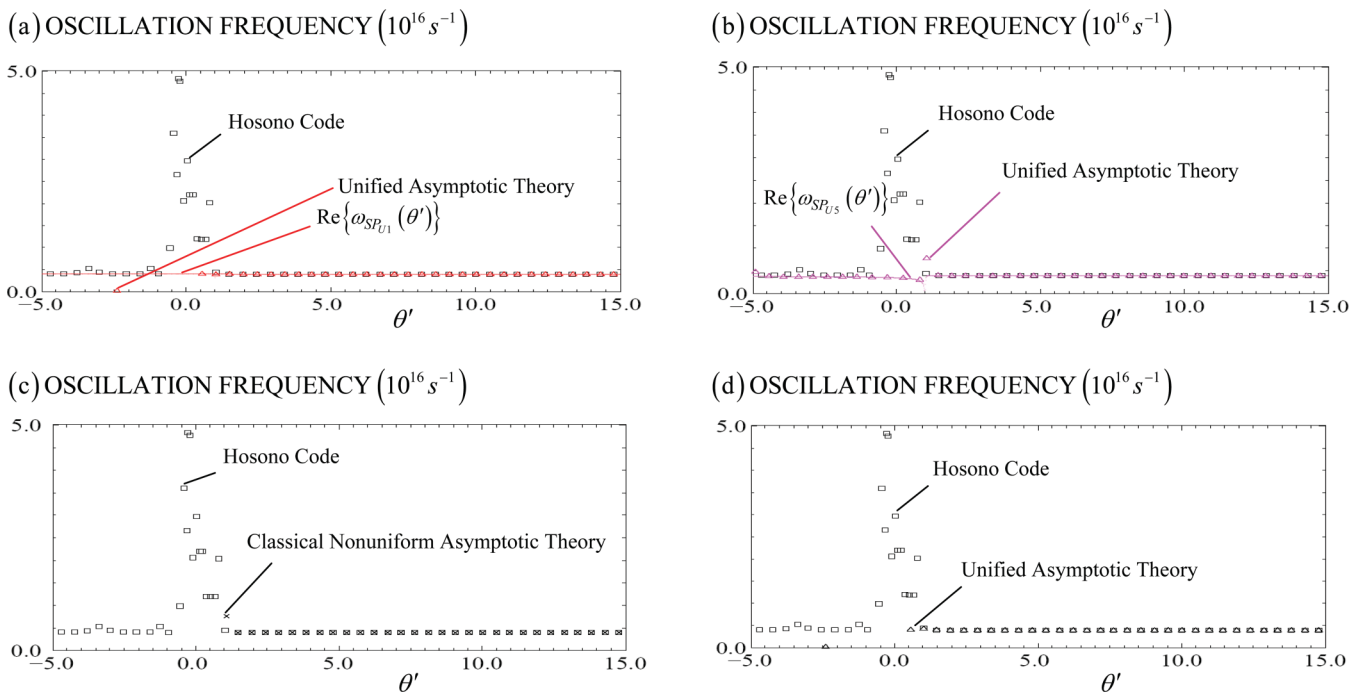

FIG. 6. (Color online) The instantaneous angular frequency of oscillation of the propagated field due to an input unit-amplitude Gaussian-modulated harmonic (sine) wave with initial pulse width $2T = 0.2$ fs and carrier frequency $\omega_c = 4.0 \times 10^{15}$ s^{-1}, at a propagation distance $z = 1.0$ μm in a single resonance Lorentz-type dispersive and gain medium. In all diagrams, the squares (online denoted in black) denote the Hosono code evaluated oscillation frequency. In (a) the triangles (online denoted in red) denote the unified asymptotic theory evaluated oscillation frequency and is due to the asymptotic contribution of the saddle point SP_{U1}. Moreover, the solid line (online denoted in red) represents the real part of the respective saddle point SP_{U1}. In (b) the triangles (online denoted in magenta) denote the unified asymptotic theory evaluated oscillation frequency and is due to the asymptotic contribution of the saddle point SP_{U5}. Moreover, the solid line (online denoted in magenta) represents the real part of the respective saddle point SP_{U5}. In (c) the crosses (online denoted in black) denote the instantaneous frequency of oscillation evaluated from the classical nonuniform asymptotic theory. In (d) the triangles (online denoted in black) denote the instantaneous frequency of oscillation evaluated from the unified asymptotic theory.

completes only 0.032 oscillations. An examination of the four cases in pairs illustrates the dependence of the propagated field dynamics on the applied carrier frequency ω_c (first and second cases), the initial pulse width $2T$ (first and third cases), and the propagation distance z (first and fourth cases). For each of these four cases, there is a corresponding diagram in Figs. 12 and 13 which illustrates the respective saddle point dynamics, as well as a corresponding diagram in Figs. 14 and 15 which illustrates the respective behavior of the real part of the unified phase function along the real frequency axis.

In each of the four cases depicted in Figs. 1–11, the results of a numerical implementation of the algorithm that was originally proposed by Hosono [37] and later improved upon by Wyns *et al.* [38] are used as a comparison with the corresponding descriptions of the propagated field dynamics afforded by the unified as well as the classical asymptotic approaches, as it was done in the case of an absorptive Lorentzian dielectric [9,30–33]. Hereafter, this purely numerical experiment is referred to as the "Hosono code" (throughout, the parameter values $a = 15$, $k = 5 \times 10^4$, and $m = 250$ [38] have been utilized). A numerical implementation of the asymptotic method of Olver [34] is also utilized in each respective case in order to evaluate the classical, exact integral expression (1) of the propagated field, employing exact, numerically determined saddle point locations and exact expressions for the derivatives of the classical phase function at these saddle points, and is referred to as the "classical nonuniform asymptotic theory." The results of this classical asymptotic approach are included here in order to demonstrate the improvements afforded by the unified asymptotic approach; the classical nonuniform asymptotic theory is nonuniform in certain θ' intervals [39]. A numerical implementation of the general expressions (11) and (12) which result from an application of Olver's method [34] to the unified, exact integral expression (6) of the propagated field is referred to here as the "unified asymptotic theory," and is also respectively implemented in each of the four cases. In this numerical implementation, exact, numerically determined saddle point locations and exact expressions for the derivatives of the unified phase function at them are also utilized. This is because the saddle point locations appear in the exponential terms of the propagated field expressions (11) and (12) and small errors in the analytical description of these locations can produce a large error in the unified asymptotic description of the propagated field in Gaussian pulse propagation [31–33]. Since the five saddle points of the unified phase function remain isolated and are all of first order for all values of θ' in the chosen single resonance Lorentz-type gain medium, the unified asymptotic theory results in a description of the propagated field dynamics that is

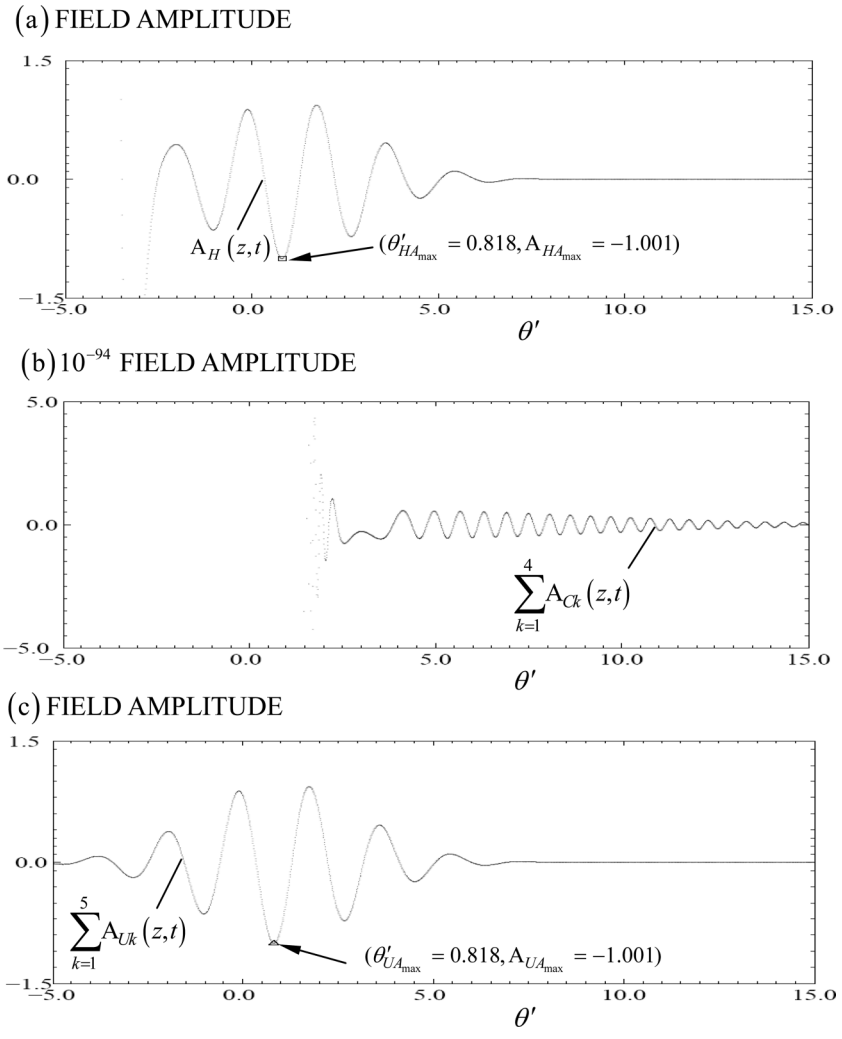

FIG. 7. The dynamical evolution of the propagated field, evaluated using (a) the Hosono code $[A_H(z,t)]$, (b) the classical nonuniform asymptotic theory $[\sum_{k=1}^{4} A_{Ck}(z,t)]$, and (c) the unified asymptotic theory $[\sum_{k=1}^{5} A_{Uk}(z,t)]$, due to an input unit-amplitude Gaussian-modulated harmonic (sine) wave with initial pulse width $2T = 20.0$ fs and carrier frequency $\omega_c = 1.0 \times 10^{15}$ s^{-1}, at a propagation distance $z = 1.0$ μm in a single resonance Lorentz-type dispersive and gain medium. Since the classical nonuniform asymptotic theory is completely inaccurate, only the square in the top diagram and the triangle in the bottom diagram denote the respective (absolute) field amplitude maxima. In the middle diagram the (total) field amplitude is due to the (algebraic sum of the) asymptotic contributions of the relevant saddle points SP_{Ck}, $k = 1,2,\ldots,4$, of the classical phase function. In the bottom diagram the (total) field amplitude is due to the asymptotic contribution of the single relevant saddle points SP_{U1} of the unified phase function.

uniformly valid with respect to θ'. In the ensuing, the Gaussian envelope of the input pulse is chosen to be centered at the time $t_0 = 3.035T$ and is considered to extend over all time. In addition, the Hosono code, as well as the unified asymptotic theory, have been used to compute the propagated field dynamics over the θ' interval $-5.0 \leqslant \theta' \leqslant +15.0$, and when necessary their respective results are depicted over this entire interval; where depicted, the classical nonuniform asymptotic theory is invoked in the θ' interval $+1.0005 \leqslant \theta' \leqslant +15.0$ in order to compute the propagated field dynamics. Finally, throughout, the instantaneous oscillation frequency of each depicted propagated field is evaluated numerically from each successive positive half oscillation of the respective propagated field amplitude and is assigned at the θ' midpoint of the corresponding half oscillation along the θ' axis.

Attention is now turned to the first case depicted in Figs. 1–3. Figure 1(a) illustrates the amplitude of the (total) propagated field $A_H(z,t)$ evaluated using the Hosono code; the squares denote the (absolute) field amplitude maxima in the vicinity of $\theta' = +1.0$ [depicted by the ordered pair $(\theta'_{HA_{\max}}, A_{HA_{\max}})$] as well as for $\theta' \gg +1.0$ [depicted by the ordered pair $(\theta'_{HB_{\max}}, A_{HB_{\max}})$]. Superimposed in Fig. 1(a) is the pulse component $A_{U1}(z,t)$ of the propagated field, which is evaluated using the unified asymptotic theory and is due to the asymptotic contribution of the saddle point SP_{U1} of $\Phi_U(\omega,\theta')$ which is relevant in the asymptotic analysis for all values of θ'. The triangles in Fig. 1(a) denote the (absolute) maxima of $A_{U1}(z,t)$ in the vicinity of $\theta' = +1.0$ [i.e., the ordered pair $(\theta'_{U1A_{\max}}, A_{U1A_{\max}})$] as well as for $\theta' \gg +1.0$ [i.e. the ordered pair $(\theta'_{U1B_{\max}}, A_{U1B_{\max}})$]. Figure 3(a) illustrates the numerically determined time evolution of the instantaneous angular frequency of oscillation of each of the propagated fields denoted in Fig. 1(a). In particular, the squares represent the instantaneous oscillation frequency $\omega_{IFO_H}(\theta')$ of the (total) propagated field $A_H(z,t)$, evaluated using the Hosono code. The triangles that are also superimposed in Fig. 3(a) denote the instantaneous oscillation frequency $\omega_{IFO_{U1}}(\theta')$ of the pulse component $A_{U1}(z,t)$, which is evaluated using the unified asymptotic theory. Finally, the solid line in Fig. 3(a) denotes the real part of the respective relevant saddle point SP_{U1}.

Figure 1(b) illustrates the pulse component $A_{U5}(z,t)$ of the propagated field, which is evaluated using the unified asymptotic theory and is due to the asymptotic contribution of the saddle point SP_{U5}, superimposed upon the (total) propagated field $A_H(z,t)$ evaluated using the Hosono code; the denoted triangles and squares depict respective (absolute) field amplitude maxima. Although $A_{U5}(z,t)$ is illustrated for all values of $\theta' \in [-5.0, +15.0]$, it should only be taken into account for values of θ' in the interval $\theta' \geqslant +0.994$ since the respective saddle point SP_{U5} of $\Phi_U(\omega,\theta')$ is relevant in the asymptotic analysis only in this θ' interval. Figure 3(b) illustrates the evolution with time of the instantaneous angular frequency of oscillation of each of the propagated fields denoted in Fig. 1(b), together with the (absolute) real part of the respective relevant saddle point SP_{U5} which is depicted by the solid line in this diagram.

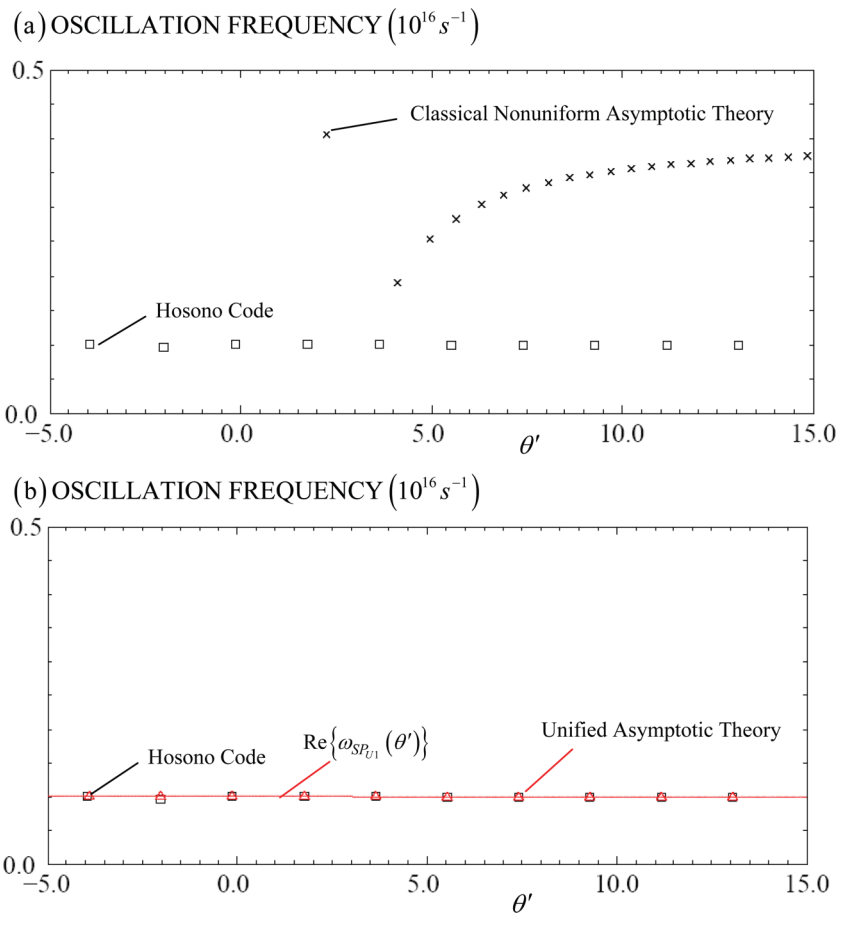

FIG. 8. (Color online) The instantaneous angular frequency of oscillation of the propagated field due to an input unit-amplitude Gaussian-modulated harmonic (sine) wave with initial pulse width $2T = 20.0$ fs and carrier frequency $\omega_c = 1.0 \times 10^{15}$ s^{-1}, at a propagation distance $z = 1.0$ μm in a single resonance Lorentz-type dispersive and gain medium. In both diagrams the squares (online denoted in black) denote the Hosono code evaluated oscillation frequency. In (a) the crosses (online denoted in black) denote the instantaneous frequency of oscillation evaluated from the classical nonuniform asymptotic theory. In (b) the triangles (online denoted in red) denote the unified asymptotic theory evaluated oscillation frequency and is due to the asymptotic contribution of the saddle point SP_{U1}. Moreover, the solid line (online denoted in red) represents the real part of the respective saddle point SP_{U1}.

Figure 2(a) illustrates the (total) propagated field $A_H(z,t)$ evaluated using the Hosono code. This is included here in order to obtain a direct comparison with Fig. 2(b) which illustrates the (total) propagated field evaluated from the classical nonuniform asymptotic theory and is due to the asymptotic contributions of the relevant saddle points SP_{Ck}, $k = 1,2,\ldots,4$, of the classical phase function, and with Fig. 2(c) which illustrates the (total) propagated field evaluated from the unified asymptotic theory using Eqs. (11) and (12) and is due to the contributions of the relevant saddle points SP_{U1} and SP_{U5} of $\Phi_U(\omega,\theta')$.

Finally, in Fig. 3(c) the crosses illustrate the time evolution of the instantaneous angular frequency of oscillation of the (total) propagated field due to the classical nonuniform asymptotic theory as depicted in Fig. 2(b), superimposed upon the corresponding instantaneous oscillation frequency denoted with squares of the (total) propagated field evaluated from the Hosono code as depicted in Fig. 2(a). Similarly, in Fig. 3(d) the triangles illustrate the evolution with time of the instantaneous angular frequency of oscillation of the (total) propagated field due to the unified asymptotic theory which is depicted in Fig. 2(c), superimposed upon the corresponding instantaneous oscillation frequency denoted with squares of the (total) propagated field evaluated from the Hosono code.

Similar considerations apply for the remaining cases depicted in Figs. 4–11. Notice that, in the second case (illustrated in Figs. 4–6) and in the fourth case (illustrated in Figs. 9–11), again the respective two saddle points SP_{U1} and SP_{U5} of $\Phi_U(\omega,\theta')$ are relevant in the asymptotic analysis of the (total) propagated field evaluated from the unified asymptotic theory. However, in the third case (illustrated in Figs. 7 and 8) only the single saddle point $SP_{U1}$of $\Phi_U(\omega,\theta')$ is relevant in the asymptotic analysis of the (total) propagated field evaluated from the unified asymptotic theory.

An inspection of the top and bottom diagrams in Figs. 2, 5, and 10 illustrates that for ultrashort Gaussian input pulses the results of the unified asymptotic theory are in excellent agreement with the respective experimental results of the Hosono code for all values of θ', except in the immediate neighborhood about $\theta' = +1.0$ when the propagated field travels nearly at the vacuum speed of light. Notice that the Hosono code breaks down for values of $\theta' < 0.0$; a detailed numerical study of the range of applicability of the Hosono code in ultrashort and/or ultrawideband dispersive pulse propagation problems is presented in Ref. [38]. As illustrated in Fig. 7, when the input Gaussian pulse is broadened, the agreement between the results of the unified asymptotic theory and the respective experimental results of the Hosono code is excellent also for values of $\theta' \leqslant +1.0$. Moreover, as illustrated in the top and middle diagrams of Figs. 2, 5, and 10, for ultrashort Gaussian input pulses the results of the classical nonuniform asymptotic theory are also in excellent agreement with the experimental results of the Hosono code and, therefore, with the respective results of the unified asymptotic theory, for all values of $\theta' > +1.0$. However, as illustrated in the top and middle diagrams of Fig. 7, when the input Gaussian pulse is broadened, the classical nonuniform asymptotic theory is incapable of providing an accurate description of the prop-

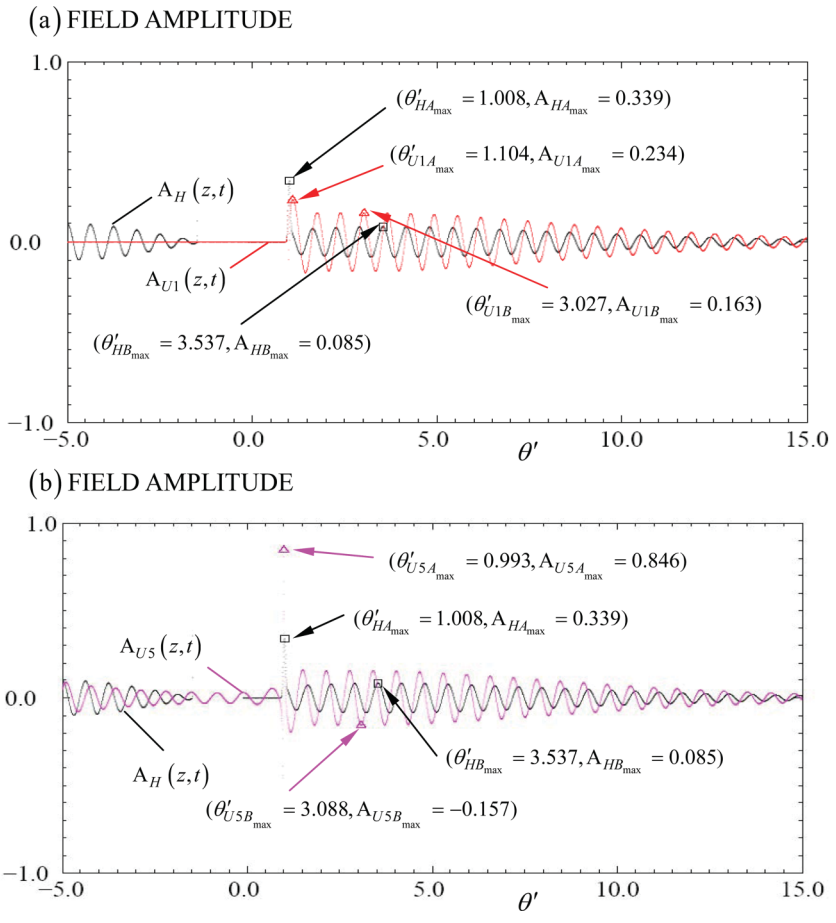

FIG. 9. (Color online) The dynamical field evolution due to an input unit-amplitude Gaussian-modulated harmonic (sine) wave with initial pulse width $2T = 0.2$ fs and carrier frequency $\omega_c = 1.0 \times 10^{15}$ s^{-1}, at a propagation distance $z = 0.75$ μm in a single resonance Lorentz-type dispersive and gain medium. In both diagrams, the solid line (online denoted in black) represents the field amplitude $A_H(z,t)$ evaluated using the Hosono code. Moreover, the squares (online denoted in black) denote (absolute) field amplitude maxima. In (a) the solid line (online denoted in red) represents the amplitude of the pulse component $A_{U1}(z,t)$ due to the asymptotic contribution of the saddle point SP_{U1} evaluated using the unified asymptotic theory. The triangles (online denoted in red) denote the respective (absolute) pulse amplitude maxima. In (b) the solid line (online denoted in magenta) represents the amplitude of the pulse component $A_{U5}(z,t)$ due to the asymptotic contribution of the saddle point SP_{U5} evaluated using the unified asymptotic theory. The triangles (online denoted in magenta) denote the respective (absolute) pulse amplitude maxima.

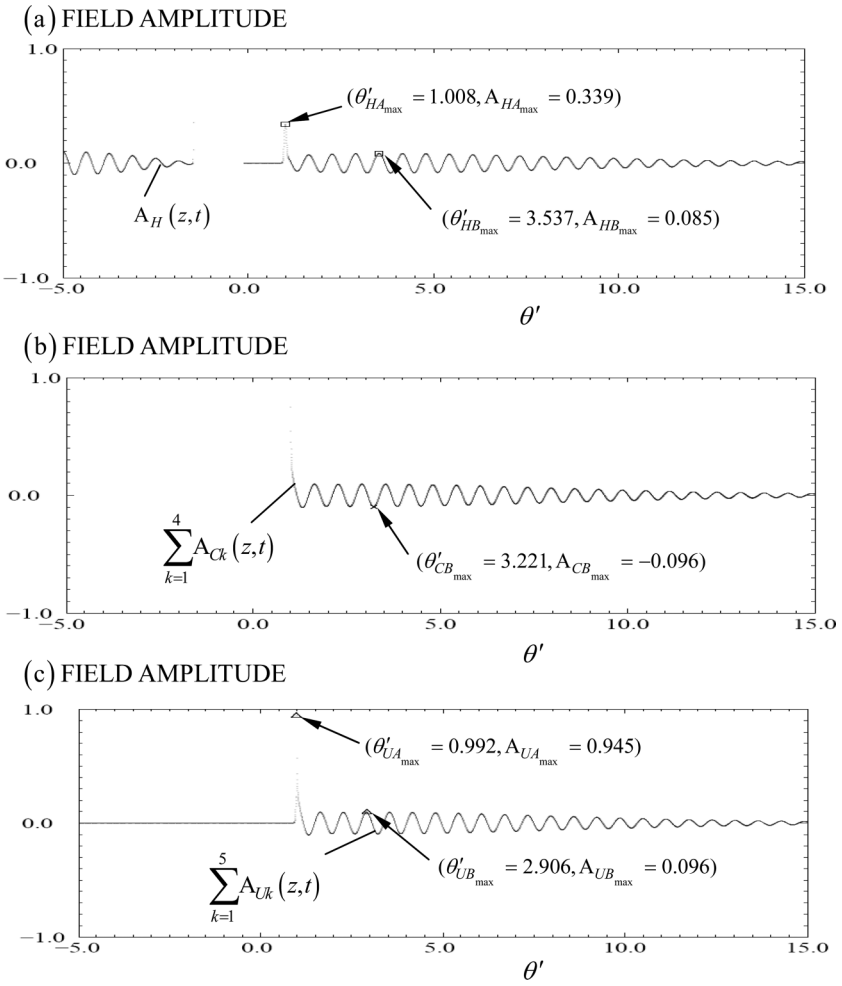

FIG. 10. The dynamical evolution of the propagated field, evaluated using (a) the Hosono code $[A_H(z,t)]$, (b) the classical nonuniform asymptotic theory $[\sum_{k=1}^{4} A_{Ck}(z,t)]$, and (c) the unified asymptotic theory $[\sum_{k=1}^{5} A_{Uk}(z,t)]$, due to an input unit-amplitude Gaussian-modulated harmonic (sine) wave with initial pulse width $2T = 0.2$ fs and carrier frequency $\omega_c = 1.0 \times 10^{15}$ s^{-1}, at a propagation distance $z = 0.75$ μm in a single resonance Lorentz-type dispersive and gain medium. The squares in the top diagram, the cross in the middle diagram, and the triangles in the bottom diagram denote (absolute) field amplitude maxima. In the middle diagram the (total) field amplitude is due to the (algebraic sum of the) asymptotic contributions of the relevant saddle points SP_{Ck}, $k = 1,2,\ldots,4$, of the classical phase function. In the bottom diagram the (total) field amplitude is due to the (algebraic sum of the) asymptotic contributions of the relevant saddle points SP_{Uk}, $k = 1,5$, of the unified phase function.

agated field as opposed to the accurate description provided by the Hosono code and the unified asymptotic theory. The high level of agreement between the unified asymptotic theory and the Hosono code is also evidenced from the diagrams in Figs. 3(d), 6(d), 8(b), and 11(d), which illustrate the respective instantaneous angular oscillation frequencies of the (total) propagated fields. Moreover, as shown in the diagrams of Figs. 3(c), 6(c), 8(a), and 11(c), which illustrate the instantaneous oscillation frequencies evaluated using the classical nonuniform asymptotic theory and the Hosono code, the classical asymptotic approach is capable of providing an accurate description of the propagated field dynamics in a gain Lorentzian medium only for ultrashort Gaussian input pulses.

Attention is next turned to each of the four cases illustrated in Figs. 1–11, combined with the corresponding diagram in Figs. 12 and 13 which illustrates the respective saddle point dynamics, as well as the corresponding diagram in Figs. 14 and 15 which illustrates the respective behavior of the real part of the unified phase function along the real frequency axis.

Consider, initially, the first case illustrated in Figs. 1–3, along with the corresponding diagrams appearing in Figs. 12(a) and 14(a). The pulse component $A_{U1}(z,t)$ $[A_{U5}(z,t)]$ of the propagated field $A(z,t)$, which is illustrated in the diagram of Fig 1(a) [Fig. 1(b)], is due to the asymptotic contribution of the saddle point $\omega_{SP_{U1}}(\theta')$ $[\omega_{SP_{U5}}(\theta')]$ which is relevant for all θ' $(\theta' \geqslant +0.994)$. According to the diagram of Fig. 3(a) [Fig. 3(b)], the evolution with time of the instantaneous angular frequency of oscillation $\omega_{IFO_{U1}}(\theta')$ $[\omega_{IFO_{U5}}(\theta')]$ of this pulse component is given almost exactly by the (absolute) real part of the respective relevant saddle point location $\mathrm{Re}\{\omega_{SP_{U1}}(\theta')\}$ $[\mathrm{Re}\{\omega_{SP_{U5}}(\theta')\}]$ as it evolves with time in the complex ω plane. This is in accordance with, thus verifying, part (I) of the unified model of Gaussian pulse propagation in a Lorentz-type dispersive and gain medium. According to the diagram of Fig. 1(a) [Fig. 1(b)], the two peak amplitudes of the pulse component $A_{U1}(z,t)$ $[A_{U5}(z,t)]$ of the propagated field occur at the respective two space-time parameter points $\theta'_{U1A_{\max}} \cong +1.086$ and $\theta'_{U1B_{\max}} \cong +4.418$ $(\theta'_{U5A_{\max}} \cong +0.995$ and $\theta'_{U5B_{\max}} \cong +4.464)$. According to Eq. (B21) the space-time points of peaks of the envelope of the pulse component $A_{U1}(z,t)$ $[A_{U5}(z,t)]$ of the propagated field occur at $\theta'_{U1A_{\mathrm{stnr}\max}} \cong +0.994$ and $\theta'_{U1B_{\mathrm{stnr}\max}} \cong +4.419$ $(\theta'_{U5A_{\mathrm{stnr}\max}} \cong +0.995$ and $\theta'_{U5B_{\mathrm{stnr}\max}} \cong +4.420)$, which is also in accordance with, thus verifying part (II) of the unified model of Gaussian pulse propagation in a Lorentz-type dispersive and gain medium. According to Fig. 12(a), the trajectory followed in the complex ω plane by the relevant saddle point $\omega_{SP_{U1}}(\theta')$ $[\omega_{SP_{U5}}(\theta')]$ intersects the real frequency axis at the real frequency value(s) $\omega_{rc_{U1}} = +0.397 \times 10^{16}$ s^{-1} $(\omega_{rc_{U5,1}} = -0.397 \times 10^{16}$ s^{-1} and $\omega_{rc_{U5,2}} = -0.136 \times 10^{16}$ s$^{-1})$, which is in excellent agreement with the local stationary points of the real part of the unified phase function along the real frequency

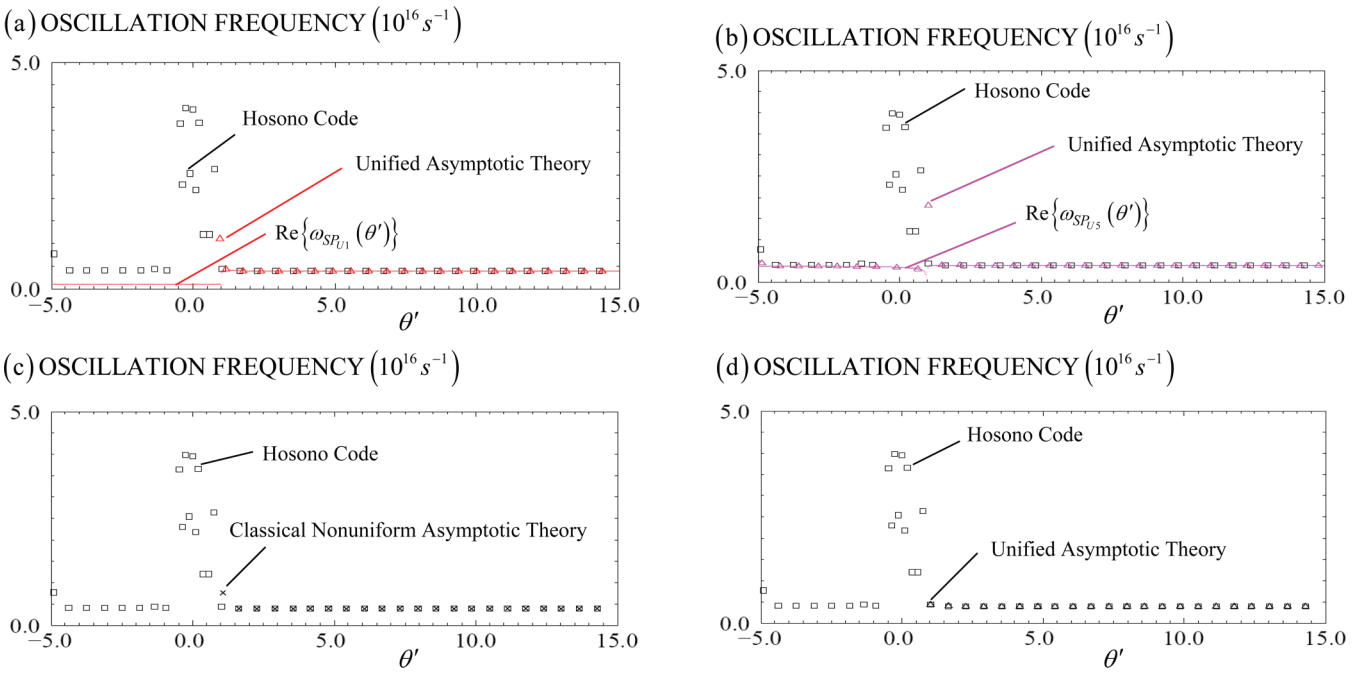

FIG. 11. (Color online) The instantaneous angular frequency of oscillation of the propagated field due to an input unit-amplitude Gaussian-modulated harmonic (sine) wave with initial pulse width $2T = 0.2$ fs and carrier frequency $\omega_c = 1.0 \times 10^{15}$ s^{-1}, at a propagation distance $z = 0.75$ μm in a single resonance Lorentz-type dispersive and gain medium. In all diagrams, the squares (online denoted in black) denote the Hosono code evaluated oscillation frequency. In (a) the triangles (online denoted in red) denote the unified asymptotic theory evaluated oscillation frequency and is due to the asymptotic contribution of the saddle point SP_{U1}. Moreover, the solid line (online denoted in red) represents the real part of the respective saddle point SP_{U1}. In (b) the triangles (online denoted in magenta) denote the unified asymptotic theory evaluated oscillation frequency and is due to the asymptotic contribution of the saddle point SP_{U5}. Moreover, the solid line (online denoted in magenta) represents the real part of the respective saddle point SP_{U5}. In (c) the crosses (online denoted in black) denote the instantaneous frequency of oscillation evaluated from the classical nonuniform asymptotic theory. In (d) the triangles (online denoted in black) denote the instantaneous frequency of oscillation evaluated from the unified asymptotic theory.

axis that are illustrated in the diagram of Fig. 14(a) and are attained at the real frequency values $\omega_{mx_1} = 0.397 \times 10^{16}$ s^{-1} ($\omega_{mx_2} = -0.397 \times 10^{16}$ s^{-1} and $\omega_{mn_1} = -0.136 \times 10^{16}$ s^{-1}); this is accordance with, and thus verifying, part (III) of the unified model of Gaussian pulse propagation in a Lorentz-type dispersive and gain medium.

Similar findings may readily be evidenced upon examining the higher applied carrier frequency case, i.e., the second case illustrated in Figs. 4–6 together with the diagrams in Figs. 12(b) and 14(b). Notice that, here, the space-time points of peaks of the envelope of the pulse component $A_{U1}(z,t)$ [$A_{U5}(z,t)$] of the propagated field occur at $\theta'_{U1A_{\mathrm{stnr}_{\max}}} \cong +0.992$ and $\theta'_{U1B_{\mathrm{stnr}_{\max}}} \cong +4.419$ ($\theta'_{U5A_{\mathrm{stnr}_{\max}}} \cong +0.997$ and $\theta'_{U5B_{\mathrm{stnr}_{\max}}} \cong +4.420$). Similar conclusions are deduced upon examining the broader input pulse case, i.e., the third case illustrated in Figs. 7 and 8 together with the diagrams in Figs. 13(a) and 15(a). Here, the space-time point of the envelope peak in the pulse component $A_{U1}(z,t)$ of the propagated field occurs at $\theta'_{U1A_{\mathrm{stnr}_{\max}}} \cong +0.961$. Finally, similar findings are evidenced upon examining the shorter propagation distance case, i.e., the fourth case illustrated in Figs. 9–11 when compared with the diagrams in Figs. 13(b) and 15(b). Here, the space-time points of envelope peaks in the pulse component $A_{U1}(z,t)$ [$A_{U5}(z,t)$] of the propagated field occur at $\theta'_{U1A_{\mathrm{stnr}_{\max}}} \cong +0.992$ and $\theta'_{U1B_{\mathrm{stnr}_{\max}}} \cong +3.045$ ($\theta'_{U5A_{\mathrm{stnr}_{\max}}} \cong +0.993$ and $\theta'_{U5B_{\mathrm{stnr}_{\max}}} \cong +3.046$).

Figures 1–11, together with Figs. 12 and 13, and Figs. 14 and 15, verify that the unified model of Gaussian pulse propagation in a Lorentz-type linear, causally dispersive and gain medium is in complete agreement with the observed dynamical evolution of the propagated field. This model extends the model of Gaussian pulse propagation of arbitrary initial pulse width which was shown to be uniformly valid in the case of a Lorentz-type dispersive and absorptive medium [9,33]. Moreover, the unified model of Gaussian pulse propagation is in agreement with the classical asymptotic description of ultrashort Gaussian pulse propagation in a Lorentz-type dispersive active medium, reducing to this classical description in the appropriate limit.

An inspection of Figs. 1–11 shows that, for the considered gain medium and for an ultrashort Gaussian input pulse, as depicted in the first (Figs. 1–3), second (Figs. 4–6), and fourth (Figs. 9–11) cases, the (total) propagated field $A(z,t)$, as well as its respective pulse components $A_{Ul}(z,t)$, $l \in N$, are each composed of a transient structure, which evolves in the vicinity of the space-time point $\theta' \cong +1.0$ traveling at nearly the vacuum speed of light, followed by a deformed Gaussian pulse structure. The transient structure in $A(z,t)$ is likely a remnant of the input ultrashort Gaussian pulse; such a spiked structure appears present at the onset of the numerically evaluated propagated field that is due to an input delta-function pulse in a single resonance Lorentz-type dispersive and absorptive

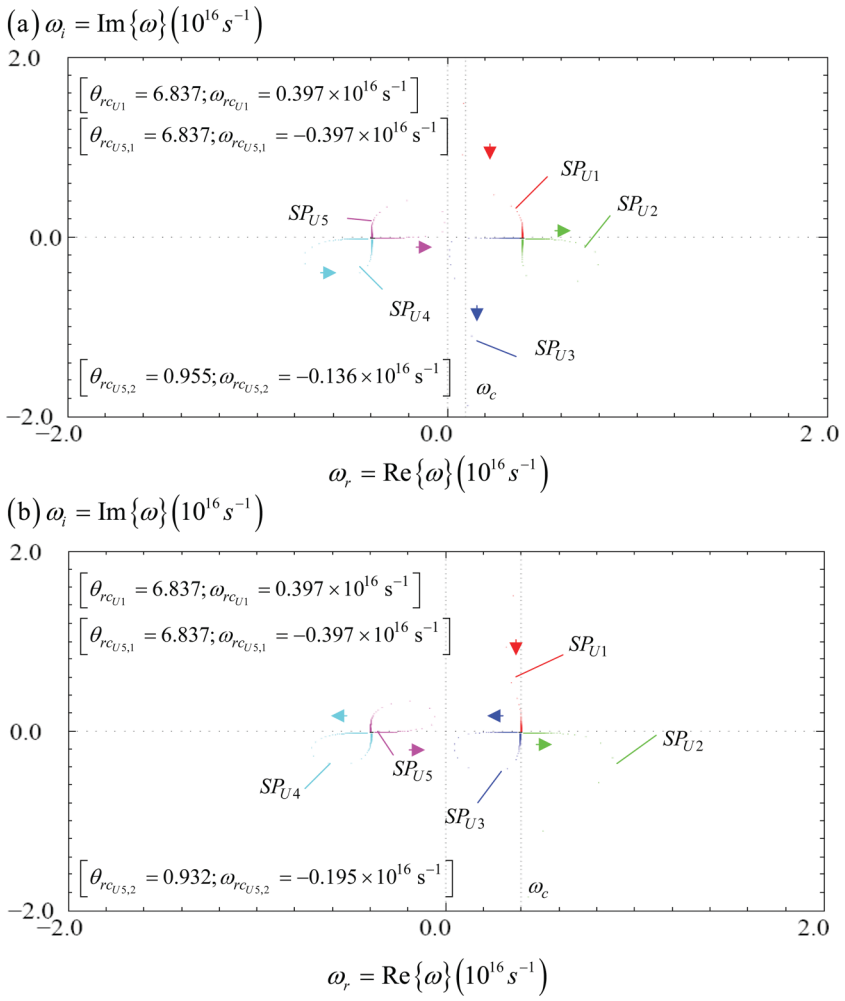

FIG. 12. (Color online) Dynamical evolution of the saddle points SP_{Uk}, $k = 1,2,\ldots,5$, of the unified phase function $\Phi_U(\omega,\theta')$ in the complex ω plane, for an input unit-amplitude Gaussian-modulated harmonic (sine) wave with initial pulse width $2T = 0.2$ fs at a propagation distance $z = 1.0\ \mu$m in the single resonance Lorentz-type dispersive and gain medium. In (a) the applied carrier frequency is $\omega_c = 1.0\times10^{15}\ \mathrm{s}^{-1}$, while in (b) the applied carrier frequency is $\omega_c = 4.0\times10^{15}\ \mathrm{s}^{-1}$. In both diagrams, the arrow at each path indicates the direction of motion of the respective saddle point as θ' increases over the domain $\theta' \in [-5.0, +15.0]$.

medium [38]. As the applied carrier frequency of the input Gaussian pulse is increased through, and then above, the amplification band of the gain medium the respective amplitude of this transient structure is increased, and then decreased, while its peak occurs at smaller values of the space-time parameter θ', traveling with higher velocities. Moreover, in the considered gain medium, the deformed Gaussian pulse structure in $A(z,t)$ exhibits similar behavior as the applied carrier frequency is increased. For such an ultrashort Gaussian input pulse, the instantaneous oscillation frequencies of the (total) propagated field $A(z,t)$, as well as of its respective pulse components $A_{Ul}(z,t)$, $l \in N$, evolve in the spectral range between the applied carrier frequency and the amplification band of the gain medium, as the space-time parameter increases away from the value $\theta' \cong +1.0$. Moreover, the pulse components $A_{Ul}(z,t)$, $l \in N$ comprising the respective (total) propagated field $A(z,t)$ are seen to be of comparable amplitudes and are phase shifted with respect to each other. As the input Gaussian pulse is broadened significantly, the (total) propagated field $A(z,t)$ becomes compact. In this case, only a deformed Gaussian pulse structure due to the asymptotic contribution of a single relevant saddle point prevails and its peak travels with velocity that may become greater than the vacuum speed of light [12,14,18,39,41]. Indeed, in Figs. 7(a) and 7(c) the peak amplitude of the (total) propagated field travels with the superluminal velocity $\upsilon_{UA_{\max}} = \frac{c}{\theta'_{UA_{\max}}} \cong \upsilon_{HA_{\max}} = \frac{c}{\theta'_{HA_{\max}}} \cong 1.223c$ in the gain Lorentzian medium. Notice that for this particular case, according to Eq. (B21), the peak (stationary point) of the envelope of the pulse component $A_{U1}(z,t)$, as well as of the (total) propagated field, travels with velocity $\upsilon_{UA_{\mathrm{stnr}_{\max}}} = \frac{c}{\theta'_{UA_{\mathrm{stnr}_{\max}}}} = \upsilon_{U1A_{\mathrm{stnr}_{\max}}} = \frac{c}{\theta'_{U1A_{\mathrm{stnr}_{\max}}}} \cong 1.041c$, which is also superluminal. Notice also that according to the approximate, heuristic analysis in Appendix C, the peak in the envelope of the pulse component $A_{R1}(z,t)$ travels with velocity $\upsilon_{\mathrm{peak}_{R1}} = \frac{c}{\theta_{\mathrm{peak}_{R1}}} \cong 0.963c$ which is subluminal and smaller than the peak envelope velocity predicted by the unified asymptotic theory; in case the term $\Delta_{2_{Ul}}(\theta')$ becomes negligible when the trajectory followed by the corresponding relevant saddle point of $\Phi_U(\omega,\theta')$ intersects the real frequency axis, which marks the space-time point when the peak (stationary point) of the envelope of the respective single pulse component occurs, then $\upsilon_{UA_{\mathrm{stnr}_{\max}}}$ approaches the velocity $\upsilon_{\mathrm{peak}_{R1}}$. As the input Gaussian pulse is broadened significantly, the instantaneous frequency of oscillation of the (total) propagated field $A(z,t)$, as well as of its single pulse component, is increasingly concentrated about the applied carrier frequency. Finally, as the propagation distance in the gain Lorentzian medium is increased, the propagated field also becomes compact; eventually, however, material nonlinearities need to be considered.

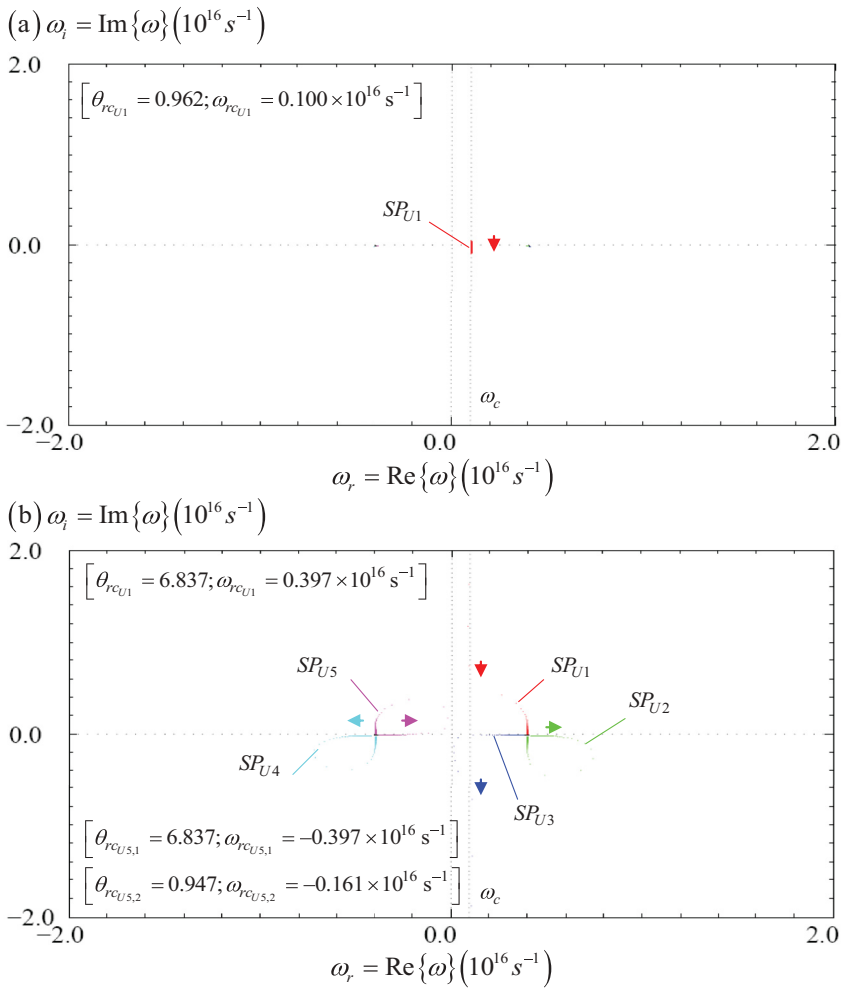

FIG. 13. (Color online) Dynamical evolution of the saddle points SP_{Uk}, $k = 1,2,\ldots,5$, of the unified phase function $\Phi_U(\omega,\theta')$ in the complex ω plane, for an input unit-amplitude Gaussian-modulated harmonic (sine) wave. In (a) the initial pulse width is $2T = 20.0$ fs, the applied carrier frequency is $\omega_c = 1.0 \times 10^{15}$ s^{-1}, and the propagation distance is $z = 1.0$ μm in the single resonance Lorentz-type dispersive and gain medium. In (b) the initial pulse width is $2T = 0.2$ fs, the applied carrier frequency is $\omega_c = 1.0 \times 10^{15}$ s^{-1}, and the propagation distance is $z = 0.75$ μm in this single resonance Lorentz-type dispersive and gain medium. Note that in the top diagram two of the five saddle points are exceedingly close to the left branch cut $\omega_-\omega'_-$, whereas two additional saddle points are exceedingly close to the right branch cut $\omega'_+\omega_+$. In both diagrams, the arrow at each path indicates the direction of motion of the respective saddle point as θ' increases over the domain $\theta' \in [-5.0, +15.0]$.

V. CONCLUSIONS

The unified asymptotic approach is employed and yields a complete, accurate, uniformly valid description of the propagated field dynamics due to an input Gaussian-modulated harmonic wave of arbitrary initial pulse width in a linear, causally dispersive gain Lorentzian medium. This asymptotic approach applies Olver's asymptotic method [9,34] on the unified exact, integral expression (6) of the propagated field, which is obtained from an appropriate rearrangement of its classical integral counterpart (1) and is characterized by a unified complex phase function $\Phi_U(\omega,\theta')$ that depends upon the input field and gain medium parameters as well as upon the propagation distance in the medium; this dependence of $\Phi_U(\omega,\theta')$ necessitates that the unified asymptotic approach must be employed each time one of these parameters changes value.

The unified asymptotic approach is uniformly valid for all values of the space-time parameter θ'. Moreover, it is uniformly valid in the propagation distance z, the gain medium parameters, as well as in the applied carrier frequency ω_c and initial width $2T$ of the input Gaussian pulse. Therefore, the resultant unified asymptotic description of the propagated field dynamics is valid for arbitrarily short or long initial pulses. Moreover, in the limit of an input ultrashort Gaussian pulse, this unified description reduces to the limiting description afforded by the classical asymptotic approach while in the opposite limit it reduces to approaches that employ the slowly varying envelope approximation. More importantly, the unified asymptotic approach leads to the unified model of Gaussian pulse propagation in a gain Lorentzian medium which extends the model that was shown to be uniformly valid for Gaussian pulse propagation of arbitrary initial pulse width in the case of a Lorentz-type dispersive and absorptive medium [9,33]. According to this model, the propagated field $A(z,t)$ is composed of pulse components $A_{Ul}(z,t)$, each being due to the asymptotic contribution of a respective relevant saddle point $\omega_{SP_{Ul}}(\theta')$ of $\Phi_U(\omega,\theta')$. The instantaneous angular frequency of oscillation $\omega_{IFO_{Ul}}(\theta')$ and the stationary point(s) of the envelope of each such pulse component are then obtained from the real and imaginary parts, respectively, of the corresponding relevant saddle point as it evolves in the complex ω plane. Therefore, this unified model directly relates the dynamics of the relevant saddle points of $\Phi_U(\omega,\theta')$ with the propagated field dynamics.

In the case of an ultrashort Gaussian input pulse, each pulse component and the respective (total) propagated field is composed of a transient structure, which evolves in the vicinity of the space-time point $\theta' \cong +1.0$ traveling at nearly the vacuum speed of light, followed by a deformed Gaussian pulse structure. In such an input pulse case, the instantaneous oscillation frequencies of each pulse component as well

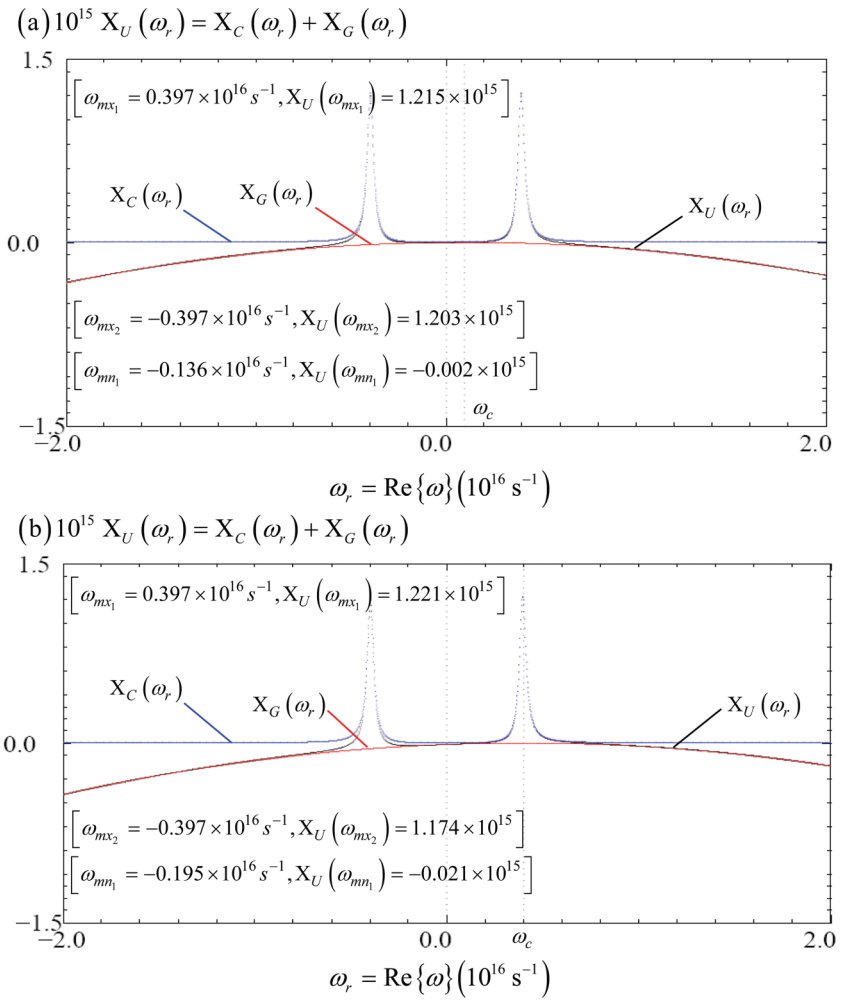

FIG. 14. (Color online) Behavior of the real part of the unified phase function $X_U(\omega_r)$ (online denoted in black), the real part of the classical phase function $X_C(\omega_r)$ (online denoted in blue), and the real part of the phase term that is due to the spectrum of the input pulse $X_G(\omega_r)$ (online denoted in red), along the real frequency axis, for an input unit-amplitude Gaussian-modulated harmonic (sine) wave with initial pulse width $2T = 0.2$ fs at a propagation distance $z = 1.0\ \mu$m in the single resonance Lorentz-type dispersive and gain medium. In (a) the applied carrier frequency is $\omega_c = 1.0\times10^{15}\ \mathrm{s}^{-1}$, while in (b) the applied carrier frequency is $\omega_c = 4.0\times10^{15}\ \mathrm{s}^{-1}$.

as of the respective (total) propagated field evolve in the spectral range between the applied carrier frequency and the amplification band of the gain medium. As the input Gaussian pulse is broadened, the propagated field $A(z,t)$ becomes compact. In this case, only a deformed Gaussian structure prevails and its peak travels with velocity that may become greater than the vacuum speed of light [12,14,18,39,41]. The instantaneous frequency of oscillation of the propagated field, is then increasingly concentrated about the applied carrier frequency.

APPENDIX A: DYNAMICS OF THE SADDLE POINTS OF THE UNIFIED PHASE FUNCTION IN THE COMPLEX ω PLANE

In a single resonance Lorentz-type dispersive and gain medium, the unified phase function $\Phi_U(\omega,\theta')$ appearing in the unified integral formulation of Gaussian pulse propagation given in Eqs. (6)–(8), is stationary at its saddle points so that their exact locations in the complex ω plane are given by the roots of the general equation

$$\frac{d\Phi_U(\omega,\theta')}{d\omega} = \left\{ i[n(\omega) - \theta'] + i\omega\frac{dn(\omega)}{d\omega} \right\} + \left[-\frac{cT^2}{2z}(\omega - \omega_c) \right] = 0. \quad \text{(A1)}$$

When the first derivative of the refractive index is substituted into Eq. (A1), the exact saddle point equation becomes

$$\left(\frac{\omega^2 - \omega_1^2 + i2\delta\omega}{\omega^2 - \omega_0^2 + i2\delta\omega}\right) - \left[\frac{\omega b^2(\omega + i\delta)}{(\omega^2 - \omega_0^2 + i2\delta\omega)^2}\right] = \left[\theta' - i\frac{cT^2}{2z}(\omega - \omega_c)\right]\left(\frac{\omega^2 - \omega_1^2 + i2\delta\omega}{\omega^2 - \omega_0^2 + i2\delta\omega}\right)^{1/2}. \quad \text{(A2)}$$

It is straightforward to show that the expression (A2) has five, in general, complex-valued roots, so that five saddle points are involved in the procedure for the asymptotic evaluation of the unified integral expression of the propagated field. According to Eq. (A2), the dynamical evolution in the complex ω plane of the five saddle points of $\Phi_U(\omega,\theta')$ depends not only upon the medium parameters but also upon the carrier frequency ω_c and the initial pulse width $2T$ of the input Gaussian-modulated harmonic wave, as well as upon the propagation distance z in the causally dispersive gain medium.

As it is difficult to determine accurate analytic expressions for the roots of the exact saddle point equation (A2), attention is initially restricted to an analytic determination of the saddle point locations in certain limiting cases. Notice that the roots of Eq. (A2), i.e., the saddle point locations, appear in the exponents of the propagated field expressions (11) and (12), which necessitates that, when derived analytically, the

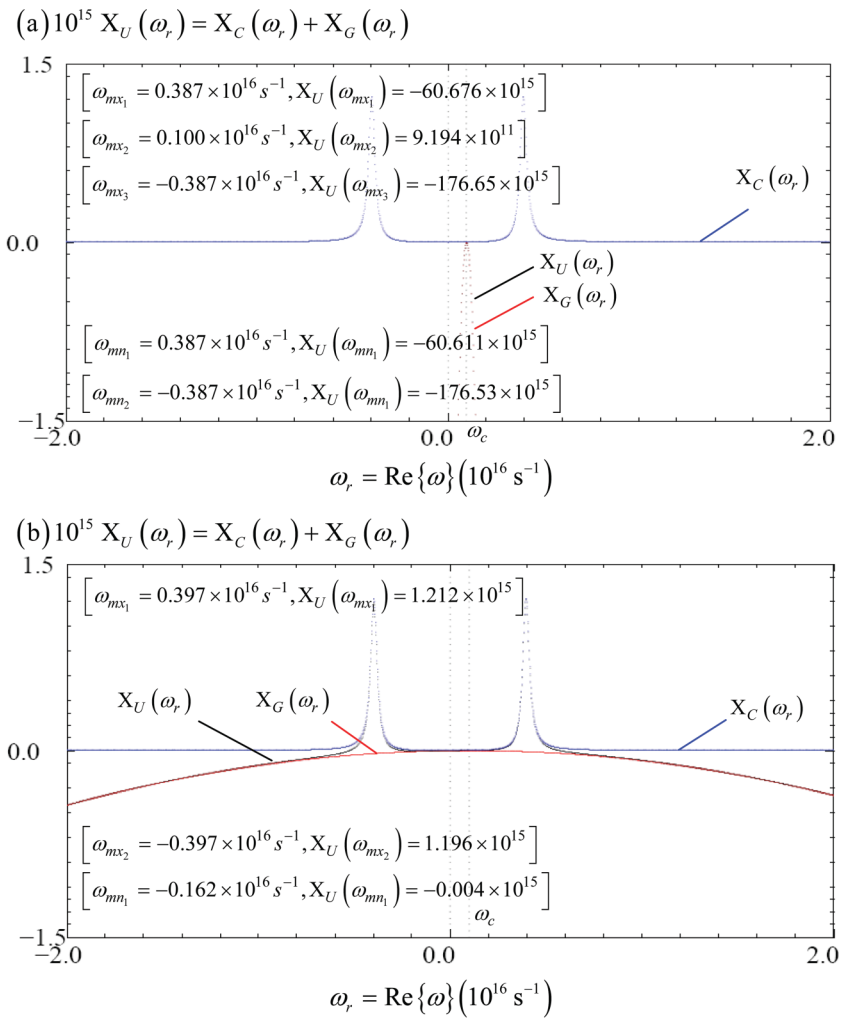

FIG. 15. (Color online) Behavior of the real part of the unified phase function $X_U(\omega_r)$ (online denoted in black), the real part of the classical phase function $X_C(\omega_r)$ (online denoted in blue), and the real part of the phase term that is due to the spectrum of the input pulse $X_G(\omega_r)$ (online denoted in red), along the real frequency axis, for an input unit-amplitude Gaussian-modulated harmonic (sine) wave. In (a) the initial pulse width is $2T = 20.0$ fs, the applied carrier frequency is $\omega_c = 1.0 \times 10^{15}\ \mathrm{s}^{-1}$, and the propagation distance is $z = 1.0\ \mu$m in the single resonance Lorentz-type dispersive and gain medium. In (b) the initial pulse width is $2T = 0.2$ fs, the applied carrier frequency is $\omega_c = 1.0 \times 10^{15}\ \mathrm{s}^{-1}$, and the propagation distance is $z = 0.75\ \mu$m in this single resonance Lorentz-type dispersive and gain medium.

respective expressions for the saddle point locations must be extremely accurate in order for the unified asymptotic approach to accurately describe the propagated field in Gaussian pulse propagation. Equation (A2) is then rewritten as

$$\left(\frac{\omega^2-\omega_1^2+i2\delta\omega}{\omega^2-\omega_0^2+i2\delta\omega}\right)^{1/2} - \left[\frac{\omega b^2(\omega+i\delta)}{(\omega^2-\omega_1^2+i2\delta\omega)^{1/2}(\omega^2-\omega_0^2+i2\delta\omega)^{3/2}}\right] + \left[i\frac{cT^2}{2z}(\omega-\omega_c)\right] = \theta', \tag{A3}$$

which shows that, as $2T$ approaches zero from above and/or as z approaches infinity, the third term appearing on the left-hand side of Eq. (A3) is negligible compared to the remaining two terms. In this case, the dynamical evolution of four of the five saddle points of the unified phase function are approximately obtained from the equation describing the dynamical evolution of the four saddle points of the classical phase function [39], to which Eq. (A3) reduces to. In this particular case, and in the limit as θ' tends to $-\infty$, four saddle points of $\Phi_U(\omega,\theta')$ emanate from the vicinity of the four branch points $\omega'_\pm$ and $\omega_\pm$ of $n(\omega)$, in the complex ω plane. In the limit as θ' tends to $+\infty$, four saddle points of $\Phi_U(\omega,\theta')$ also approach these four branch points of $n(\omega)$ [39]. On the other hand, as $2T$ approaches infinity and/or as z approaches zero from above, the first two terms appearing on the left-hand side of Eq. (A3) are negligible compared to the third term, except at the four branch points of $n(\omega)$. In this case, the dynamical evolution of one of the five saddle points of the unified phase function may approximately be obtained from the relation

$$i\frac{cT^2}{2z}(\omega-\omega_c) = -\frac{cT^2\omega_i}{2z} + i\frac{cT^2}{2z}(\omega_r-\omega_c) = \theta'. \tag{A4}$$

Therefore, in the limit as θ' tends to $-\infty$, one saddle point asymptotically approaches the line $\omega = \omega_c$ towards the point $\omega_c + i\infty$ in the complex ω plane. Moreover, in the limit as θ' tends to $+\infty$, one saddle point asymptotically approaches the line $\omega = \omega_c$ towards the point $\omega_c - i\infty$ in the complex ω plane.

Figures 12 and 13, which depict the results of a numerical solution of the exact saddle point equation (A2), illustrate the dependence of the saddle point dynamics on the carrier frequency ω_c [compare the diagrams in Figs. 12(a) and 12(b)], the initial pulse width $2T$ [compare the diagrams in Figs. 12(a) and 13(a)], and the propagation distance z [compare the diagrams in Figs. 12(a) and 13(b)]. In each figure, the saddle

points SP_{Uk}, $k = 1,2,\ldots,5$, are numbered in a clockwise fashion with SP_{U1} denoting the saddle point which originates at $\omega_c + i\infty$ in the complex ω plane as θ' tends to $-\infty$ and has the line $\omega = \omega_c$ as its asymptote. The arrow appearing at the path traversed by a particular saddle point indicates the direction of motion of this saddle point as the parameter θ' increases over the domain $\theta' \in [-5.0, +15.0]$. In each figure the quantities $\theta_{rc_{Uk,m}}$ and $\omega_{rc_{Uk,m}}$, $k,m \in N$, denote the real space-time parameter value and the real frequency value, respectively, where the trajectory followed by the saddle point SP_{Uk} intersects the real frequency axis; the first subscript $k \in N$ characterizes the saddle point SP_{Uk}, whereas the second subscript $m \in N$, whenever present, characterizes successive points where the trajectory followed by the respective saddle point intersects the real frequency axis. This numerical study verifies that, for a single resonance Lorentz-type dispersive and gain medium, $\Phi_U(\omega,\theta')$ has five saddle points whose dynamical evolution in the complex ω plane exhibits a limiting behavior which is in complete agreement with the preceding analytic considerations.

APPENDIX B: DERIVATION OF THE UNIFIED MODEL OF GAUSSIAN PULSE PROPAGATION IN A LORENTZ-TYPE DISPERSIVE AND GAIN MEDIUM

By definition, at each of the isolated, first-order saddle points, SP_{Uk}, $k = 1,2,\ldots,5$, of the unified phase function $\Phi_U(\omega,\theta')$, which are the only saddle points that may be relevant in the asymptotic analysis for any given value of θ', the set of equations [34]

$$\left.\frac{d\Phi_U(\omega,\theta')}{d\omega}\right|_{\omega=\omega_{SP_{Uk}}} = 0 \tag{B1}$$

and

$$\left.\frac{d^2\Phi_U(\omega,\theta')}{d\omega^2}\right|_{\omega=\omega_{SP_{Uk}}} \neq 0 \tag{B2}$$

is always satisfied. Equation (B1) yields the set of equations [42]

$$\left.\frac{\partial X_U(\omega_r,\omega_i,\theta')}{\partial\omega_r}\right|_{\omega=\omega_{SP_{Uk}}} = \left.\frac{\partial Y_U(\omega_r,\omega_i,\theta')}{\partial\omega_i}\right|_{\omega=\omega_{SP_{Uk}}} = 0 \tag{B3}$$

and

$$\left.\frac{\partial X_U(\omega_r,\omega_i,\theta')}{\partial\omega_i}\right|_{\omega=\omega_{SP_{Uk}}} = -\left.\frac{\partial Y_U(\omega_r,\omega_i,\theta')}{\partial\omega_r}\right|_{\omega=\omega_{SP_{Uk}}} = 0 \tag{B4}$$

for any given value of θ'; the saddle points SP_{Uk} are contained in the domain D of the complex ω plane where $\Phi_U(\omega,\theta')$ is analytic. At each of the isolated, first-order relevant saddle points SP_{Uk}, $k = 1,2,\ldots,5$, the second derivative of the unified phase function appearing in Eqs. (11) and (12) may be written as

$$\frac{d^2\Phi_U(\omega_{SP_{Uk}},\theta')}{d\omega^2} \equiv \left.\frac{d^2\Phi_U(\omega,\theta')}{d\omega^2}\right|_{\omega=\omega_{SP_{Uk}}} = \left[\frac{\partial^2 X_U(\omega_r,\omega_i,\theta')}{\partial\omega_r^2} + i\frac{\partial^2 Y_U(\omega_r,\omega_i,\theta')}{\partial\omega_r^2}\right]_{\omega=\omega_{SP_{Uk}}} \neq 0, \tag{B5}$$

and is nonzero for any given value of θ'.

Consider the θ' interval $\Delta\theta_{Ul}$ when the pulse component $A_{Ul}(z,t)$ of the propagated field $A(z,t)$ is due to the asymptotic contribution of the relevant saddle point $\omega_{SP_{Ul}}(\theta')$ of $\Phi_U(\omega,\theta')$. In this θ' interval the instantaneous frequency of oscillation $\omega_{IFO_{Ul}}(\theta')$ of $A_{Ul}(z,t)$ may be obtained from the time derivative of the oscillatory phase term in Eq. (12) as [9,20,33]

$$\begin{aligned}-\omega_{IFO_{Ul}}(\theta') &= \frac{d}{dt}\left(\frac{z}{c}Y_U\left(\omega^r_{SP_{Ul}}(\theta'),\omega^i_{SP_{Ul}}(\theta'),\theta'\right)\right.\\ &\quad\left.-\frac{1}{2}\left\{\arg\left[\frac{d^2\Phi_U\left(\omega_{SP_{Ul}}(\theta'),\theta'\right)}{d\omega^2}\right]+\pi\right\}\right)\\ &= \frac{d}{d\theta'}\left[Y_U\left(\omega^r_{SP_{Ul}}(\theta'),\omega^i_{SP_{Ul}}(\theta'),\theta'\right)\right]\\ &\quad-\frac{1}{2}\frac{d}{dt}\left\{\arg\left[\frac{d^2\Phi_U\left(\omega_{SP_{Ul}}(\theta'),\theta'\right)}{d\omega^2}\right]\right\}.\end{aligned} \tag{B6}$$

Hereafter, the notation $\omega^r_{SP_{Ul}}(\theta') \equiv \mathrm{Re}\{\omega_{SP_{Ul}}(\theta')\}$ represents the real part, while the notation $\omega^i_{SP_{Ul}}(\theta') \equiv \mathrm{Im}\{\omega_{SP_{Ul}}(\theta')\}$ represents the imaginary part of the relevant saddle point $\omega_{SP_{Ul}}(\theta')$. The first term on the right-hand side of Eq. (B6) is given by

$$\begin{aligned}&\frac{d}{d\theta'}\left[Y_U\left(\omega^r_{SP_{Ul}}(\theta'),\omega^i_{SP_{Ul}}(\theta'),\theta'\right)\right]\\ &\quad= \frac{\partial Y_U\left(\omega^r_{SP_{Ul}},\omega^i_{SP_{Ul}},\theta'\right)}{\partial\theta'} = -\omega^r_{SP_{Ul}}(\theta') = -\mathrm{Re}\left\{\omega_{SP_{Ul}}(\theta')\right\},\end{aligned} \tag{B7}$$

where use was made of the relations (B3) and (B4) and of the expression for the imaginary part of the unified phase function given in Eq. (C4).

The second term on the right-hand side of Eq. (B6) is given by

$$\frac{1}{2}\frac{d}{dt}\left\{\arg\left[\frac{d^2\Phi_U\left(\omega_{SP_{Ul}}(\theta'),\theta'\right)}{d\omega^2}\right]\right\} = \Delta_{1_{Ul}}(\theta'), \tag{B8}$$

and is always finite. Here, the term $\Delta_{1_{Ul}}(\theta')$ is given by

$$\Delta_{1_{Ul}}(\theta') = \frac{N_{\Delta_{1_{Ul}}}(\theta')}{D_{\Delta_{1_{Ul}}}(\theta')}, \tag{B9}$$

where

$$N_{\Delta_{1_{UI}}}(\theta') = \frac{d}{d\theta'}\left[\frac{\partial^2 Y_U(\omega_r,\omega_i,\theta')}{\partial\omega_r^2}\bigg|_{\omega=\omega_{SP_{UI}}(\theta')}\right]\frac{\partial^2 X_U(\omega_r,\omega_i,\theta')}{\partial\omega_r^2}\bigg|_{\omega=\omega_{SP_{UI}}} - \frac{d}{d\theta'}\left[\frac{\partial^2 X_U(\omega_r,\omega_i,\theta')}{\partial\omega_r^2}\bigg|_{\omega=\omega_{SP_{UI}}(\theta')}\right]\frac{\partial^2 Y_U(\omega_r,\omega_i,\theta')}{\partial\omega_r^2}\bigg|_{\omega=\omega_{SP_{UI}}} \tag{B10}$$

and

$$D_{\Delta_{1_{UI}}}(\theta') = \frac{2z}{c}\left|\frac{d^2\Phi_U\left(\omega_{SP_{UI}},\theta'\right)}{d\omega^2}\right|^2. \tag{B11}$$

Substitution of Eqs. (B7) and (B8) into Eq. (B6) yields

$$\omega_{IFO_{UI}}(\theta') = \mathrm{Re}\left\{\omega_{SP_{UI}}(\theta')\right\} + \Delta_{1_{UI}}(\theta'), \tag{B12}$$

where $\Delta_{1_{UI}}(\theta') = O(1/z)$ as $z \to +\infty$. When the term $\Delta_{1_{UI}}(\theta')$ becomes (asymptotically) negligible in comparison to $\mathrm{Re}\{\omega_{SP_{UI}}(\theta')\}$, then the evolution with time of the instantaneous angular frequency of oscillation $\omega_{IFO_{UI}}(\theta')$ is given by the real part of the respective relevant saddle point location $\mathrm{Re}\{\omega_{SP_{UI}}(\theta')\}$ as it evolves in the complex ω plane. This then proves part (I) of the unified model of Gaussian pulse propagation in a gain Lorentzian medium.

In this θ' interval the envelope of the pulse component $A_{UI}(z,t)$ exhibits its stationary point(s) when its first derivative with respect to time vanishes, so that

$$\begin{aligned}&\frac{d}{dt}\left\{\left|\frac{d^2\Phi_U\left(\omega_{SP_{UI}}(\theta'),\theta'\right)}{d\omega^2}\right|^{-1/2}\exp\left[\frac{z}{c}X_U\left(\omega^r_{SP_{UI}}(\theta'),\omega^i_{SP_{UI}}(\theta'),\theta'\right)\right]\right\}\\ &= \frac{d}{dt}\left[\left|\frac{d^2\Phi_U\left(\omega_{SP_{UI}}(\theta'),\theta'\right)}{d\omega^2}\right|^{-1/2}\right]\exp\left[\frac{z}{c}X_U\left(\omega^r_{SP_{UI}}(\theta'),\omega^i_{SP_{UI}}(\theta'),\theta'\right)\right]\\ &\quad + \left|\frac{d^2\Phi_U\left(\omega_{SP_{UI}},\theta'\right)}{d\omega^2}\right|^{-1/2}\frac{d}{dt}\left\{\exp\left[\frac{z}{c}X_U\left(\omega^r_{SP_{UI}}(\theta'),\omega^i_{SP_{UI}}(\theta'),\theta'\right)\right]\right\} = 0.\end{aligned} \tag{B13}$$

The first, first-order time derivative appearing on the right-hand side of Eq. (B13) is given by

$$\frac{d}{dt}\left[\left|\frac{d^2\Phi_U\left(\omega_{SP_{UI}}(\theta'),\theta'\right)}{d\omega^2}\right|^{-1/2}\right] = -\left|\frac{d^2\Phi_U\left(\omega_{SP_{UI}},\theta'\right)}{d\omega^2}\right|^{-1/2}\Delta_{2_{UI}}(\theta'), \tag{B14}$$

and is always finite. Here, the term $\Delta_{2_{UI}}(\theta')$ is given by

$$\Delta_{2_{UI}}(\theta') = \frac{N_{\Delta_{2_{UI}}}(\theta')}{D_{\Delta_{2_{UI}}}(\theta')}, \tag{B15}$$

where

$$N_{\Delta_{2_{UI}}}(\theta') = \frac{d}{d\theta'}\left[\frac{\partial^2 X_U(\omega_r,\omega_i,\theta')}{\partial\omega_r^2}\bigg|_{\omega=\omega_{SP_{UI}}(\theta')}\right]\frac{\partial^2 X_U(\omega_r,\omega_i,\theta')}{\partial\omega_r^2}\bigg|_{\omega=\omega_{SP_{UI}}} + \frac{d}{d\theta'}\left[\frac{\partial^2 Y_U(\omega_r,\omega_i,\theta')}{\partial\omega_r^2}\bigg|_{\omega=\omega_{SP_{UI}}(\theta')}\right]\frac{\partial^2 Y_U(\omega_r,\omega_i,\theta')}{\partial\omega_r^2}\bigg|_{\omega=\omega_{SP_{UI}}} \tag{B16}$$

and

$$D_{\Delta_{2_{UI}}}(\theta') = \frac{2z}{c}\left|\frac{d^2\Phi_U\left(\omega_{SP_{UI}},\theta'\right)}{d\omega^2}\right|^2. \tag{B17}$$

The second, first-order time derivative appearing on the right-hand side of Eq. (B13) is given by

$$\frac{d}{dt}\left\{\exp\left[\frac{z}{c}X_U\left(\omega^r_{SP_{UI}}(\theta'),\omega^i_{SP_{UI}}(\theta'),\theta'\right)\right]\right\} = \exp\left[\frac{z}{c}X_U\left(\omega^r_{SP_{UI}},\omega^i_{SP_{UI}},\theta'\right)\right]\frac{\partial X_U\left(\omega^r_{SP_{UI}},\omega^i_{SP_{UI}},\theta'\right)}{\partial\theta'}, \tag{B18}$$

where use was made of the relations (B3) and (B4).

Substitution of the expression for the real part of the unified phase function, which is given in Eq. (C3), into Eq. (B18) yields

$$\frac{d}{dt}\left\{\exp\left[\frac{z}{c}X_U\left(\omega^r_{SP_{Ul}}(\theta'),\omega^i_{SP_{Ul}}(\theta'),\theta'\right)\right]\right\} = \exp\left[\frac{z}{c}X_U\left(\omega^r_{SP_{Ul}},\omega^i_{SP_{Ul}},\theta'\right)\right]\omega^i_{SP_{Ul}}(\theta') = \exp\left[\frac{z}{c}X_U\left(\omega^r_{SP_{Ul}},\omega^i_{SP_{Ul}},\theta'\right)\right]\mathrm{Im}\{\omega_{SP_{Ul}}(\theta')\}. \quad \text{(B19)}$$

Substitution of Eqs. (B14) and (B19) into Eq. (B13) then yields

$$\left\{\left|\frac{d^2\Phi_U\left(\omega_{SP_{Ul}},\theta'\right)}{d\omega^2}\right|^{-1/2}\exp\left[\frac{z}{c}X_U\left(\omega^r_{SP_{Ul}},\omega^i_{SP_{Ul}},\theta'\right)\right]\right\} \times [-\Delta_{2_{Ul}}(\theta') + \mathrm{Im}\{\omega_{SP_{Ul}}(\theta')\}] = 0. \quad \text{(B20)}$$

The stationary point(s) of the envelope of the pulse component $A_{Ul}(z,t)$ occur when

$$\mathrm{Im}\{\omega_{SP_{Ul}}(\theta')\} = \Delta_{2_{Ul}}(\theta'), \quad \text{(B21)}$$

where $\Delta_{2_{Ul}}(\theta') = O(1/z)$ as $z \to +\infty$. When the term $\Delta_{2_{Ul}}(\theta')$ becomes (asymptotically) negligible, the term $\mathrm{Im}\{\omega_{SP_{Ul}}(\theta')\}$ becomes vanishingly small, in which case the stationary point(s) of the envelope of $A_{Ul}(z,t)$ occur when the trajectory followed by the respective relevant saddle point $\omega_{SP_{Ul}}(\theta')$ intersects the real frequency axis in the complex ω plane. This then proves part (II) of the unified model of Gaussian pulse propagation in a gain Lorentzian medium.

Let $\theta_{rc_{Ul}} = \theta_{\mathrm{stnr}_{Ul}}$ denote the value of θ' in the interval $\Delta\theta_{Ul}$ when the trajectory followed in the complex ω plane by the relevant saddle point $\omega_{SP_{Ul}}(\theta')$ of $\Phi_U(\omega,\theta')$ intersects the real frequency axis at the real frequency denoted by $\omega_{rc_{Ul}} = \omega_{\mathrm{stnr}_{Ul}}$, so that

$$\omega_{\mathrm{stnr}_{Ul}} \equiv \omega_{SP_{Ul}}\left(\theta_{\mathrm{stnr}_{Ul}}\right). \quad \text{(B22)}$$

From Eqs. (B3), (C2), and (C7) one readily obtains

$$\left.\frac{\partial X_U(\omega_r,\omega_i,\theta')}{\partial\omega_r}\right|_{\omega=\omega_{SP_{Ul}}(\theta_{\mathrm{stnr}_{Ul}})=\omega_{\mathrm{stnr}_{Ul}}} = \left.\frac{\partial X_U(\omega_r)}{\partial\omega_r}\right|_{\omega_r=\omega_{\mathrm{stnr}_{Ul}}=\omega_{SP_{Ul}}(\theta_{\mathrm{stnr}_{Ul}})} = 0. \quad \text{(B23)}$$

According to the second equality in Eq. (B23), the intersection point $\omega_{\mathrm{stnr}_{Ul}} = \omega_{SP_{Ul}}(\theta_{\mathrm{stnr}_{Ul}})$ is a stationary point (i.e., either a local maximum or a local minimum) of the real part of the unified phase function along the real frequency axis, i.e., it is a stationary point of the function $X_U(\omega_r)$. This then proves part (III) in the unified model of Gaussian pulse propagation in a gain Lorentzian medium.

APPENDIX C: ANALYSIS OF THE REAL PART OF THE UNIFIED PHASE FUNCTION ALONG THE REAL FREQUENCY AXIS AND APPROXIMATE, HEURISTIC EVALUATION OF GAUSSIAN PULSE PROPAGATION IN A GAIN LORENTZIAN MEDIUM

For an input Gaussian-modulated harmonic wave of arbitrary initial pulse width propagating in a single resonance Lorentz-type dispersive and gain medium, it is easy to show that the unified phase function $\Phi_U(\omega,\theta')$ appearing in Eq. (6) is not symmetric about the imaginary frequency axis and must be determined separately in any desired region of the complex ω plane. However, both $\Phi_U(\omega,\theta')$ and the refractive index $n(\omega)$ are analytic everywhere in the complex ω plane except at the four branch points $\omega'_{\pm}$ and $\omega_{\pm}$ of $n(\omega)$. In the gain medium, the expression of $\Phi_U(\omega,\theta')$ given in Eq. (8) may be separated into its real and imaginary parts as

$$\Phi_U(\omega,\theta') = i(\omega_r + i\omega_i)[n_r(\omega_r,\omega_i) - \theta' + in_i(\omega_r,\omega_i)] - \frac{cT^2}{4z}[(\omega_r-\omega_c)+i\omega_i]^2 \quad \text{(C1)}$$

$$= -\left\{\omega_r n_i(\omega_r,\omega_i) + \omega_i[n_r(\omega_r,\omega_i)-\theta'] + \frac{cT^2}{4z}\left[(\omega_r-\omega_c)^2-\omega_i^2\right]\right\} + i\left\{\omega_r[n_r(\omega_r,\omega_i)-\theta'] - \omega_i n_i(\omega_r,\omega_i) - \frac{cT^2}{2z}\omega_i(\omega_r-\omega_c)\right\}, \quad \text{(C2)}$$

so that the real part of $\Phi_U(\omega,\theta')$ is given by

$$\mathrm{Re}\{\Phi_U(\omega,\theta')\} \equiv X_U(\omega_r,\omega_i,\theta') = -\left\{\omega_r n_i(\omega_r,\omega_i) + \omega_i[n_r(\omega_r,\omega_i)-\theta'] + \frac{cT^2}{4z}\left[(\omega_r-\omega_c)^2-\omega_i^2\right]\right\}, \quad \text{(C3)}$$

and its imaginary part is given by

$$\mathrm{Im}\{\Phi_U(\omega,\theta')\} \equiv Y_U(\omega_r,\omega_i,\theta') = \omega_r[n_r(\omega_r,\omega_i)-\theta'] - \omega_i n_i(\omega_r,\omega_i) - \frac{cT^2}{2z}\omega_i(\omega_r-\omega_c). \quad \text{(C4)}$$

In Eqs (C1)–(C4), $\omega_r = \mathrm{Re}\{\omega\}$ and $\omega_i = \mathrm{Im}\{\omega\}$, while the terms $n_r(\omega_r,\omega_i)$ and $n_i(\omega_r,\omega_i)$ denote the real and imaginary parts, respectively, of $n(\omega)$.

The refractive index may be expressed in the form

$$n(\omega) = \left[1 + \frac{b^4 + 2b^2\left(\omega_r^2-\omega_i^2-\omega_0^2-2\delta\omega_i\right)}{\left(\omega_r^2-\omega_i^2-\omega_0^2-2\delta\omega_i\right)^2 + 4\omega_r^2(\omega_i+\delta)^2}\right]^{1/4}\exp\left[i\frac{\zeta(\omega_r,\omega_i)}{2}\right], \quad \text{(C5)}$$

where the function $\zeta(\omega_r,\omega_i)$ appearing in the argument of $n(\omega)$ is given by

$$\zeta(\omega_r,\omega_i) = \arctan\left[\frac{-2\omega_r b^2(\omega_i+\delta)}{\left(\omega_r^2-\omega_i^2-\omega_0^2-2\delta\omega_i\right)^2+b^2\left(\omega_r^2-\omega_i^2-\omega_0^2-2\delta\omega_i\right)+4\omega_r^2(\omega_i+\delta)^2}\right] \tag{C6}$$

and is chosen to lie in the interval $-\pi \leqslant \zeta(\omega_r,\omega_i) < \pi$. In a causal medium, the real part of the index of refraction $\mathrm{Re}\{n(\omega)\}$ is symmetric while its imaginary part $\mathrm{Im}\{n(\omega)\}$ is antisymmetric about the imaginary frequency axis [43]; it is sufficient to examine the behavior of $n(\omega)$ in the right half of the complex ω plane alone [39].

Along the real frequency axis, the real part of the unified phase function is given by

$$\begin{aligned} X_U(\omega_r) &= X_C(\omega_r) + X_G(\omega_r) \\ &= [-\omega_r n_i(\omega_r)] + \left[-\frac{cT^2}{4z}(\omega_r-\omega_c)^2\right], \end{aligned} \tag{C7}$$

where

$$X_C(\omega_r) = -\omega_r n_i(\omega_r) \tag{C8}$$

denotes the real part of the classical phase function evaluated along the real frequency axis, and where

$$X_G(\omega_r) = -\frac{cT^2}{4z}(\omega_r-\omega_c)^2 \tag{C9}$$

denotes the real part of the phase term that is due to the spectrum of the input Gaussian pulse evaluated along the same axis. According to Eq. (C7), along the real frequency axis $X_U(\omega_r)$ is independent of the space-time parameter θ'; it depends only upon the input field and gain medium parameters as well as upon the propagation distance in the medium. The behavior of $X_U(\omega_r)$ may now be determined from the behavior of the separate terms $X_C(\omega_r)$ and $X_G(\omega_r)$ appearing in Eq. (C7).

The exact locations for the stationary (local maxima and local minima) points of $X_U(\omega_r)$ are specified by the relation

$$\frac{d\Phi_U(\omega_r,\theta')}{d\omega_r} = \frac{\partial X_U(\omega_r)}{\partial\omega_r} + i\frac{\partial Y_U(\omega_r,\theta')}{\partial\omega_r} = 0, \tag{C10}$$

which, upon substitution of Eqs. (C3) and (C4) evaluated along the real frequency axis, gives

$$\frac{\partial X_U(\omega_r)}{\partial\omega_r} = -n_i(\omega_r) - \omega_r\frac{\partial n_i(\omega_r)}{\partial\omega_r} - \frac{cT^2}{2z}(\omega_r-\omega_c) = 0 \tag{C11}$$

and

$$\begin{aligned} \frac{\partial Y_U(\omega_r,\theta')}{\partial\omega_r} &= \frac{\partial}{\partial\omega_r}[\omega_r n_r(\omega_r)] - \theta' \\ &= n_r(\omega_r) + \omega_r\frac{\partial n_r(\omega_r)}{\partial\omega_r} - \theta' = 0. \end{aligned} \tag{C12}$$

The desired, exact locations of the stationary points of $X_U(\omega_r)$ are now given by the roots of Eq. (C11). When the analytic expressions for the real $[n_r(\omega_r)]$ and imaginary $[n_i(\omega_r)]$ parts of the index of refraction along the real frequency axis are substituted in Eq. (C11), the resultant expression for the exact locations of the stationary points of $X_U(\omega_r)$ is intractable analytically; however, it can be accurately solved using numerical techniques. Figures 14 and 15, depict the locations of the stationary points of $X_U(\omega_r)$ for the same input field and gain medium parameters as well as the same propagation distances in the medium utilized in Figs. 12 and 13, and provide an illustration of the dependence of the dynamics of these stationary points on the carrier frequency ω_c [compare the diagrams in Figs. 14(a) and 14(b)], the initial pulse width $2T$ [compare the diagrams in Figs. 14(a) and 15(a)], and the propagation distance z [compare Figs. 14(a) and 15(b)].

For the chosen single resonance Lorentz gain medium, $X_U(\omega_r)$ may exhibit at most five stationary points (up to three local maxima $\omega_{mx_{1,2,3}}$ and up to three local minima $\omega_{mn_{1,2,3}}$) along the real frequency axis. In particular, for any applied carrier frequency $\omega_c \geqslant 0$, $X_U(\omega_r)$ always exhibits two local maxima along the real frequency axis which, approximately, occur at the real frequencies $\omega_{\max}^+$ and $\omega_{\max}^-$ where the term $X_C(\omega_r)$ attains its maximum values along this axis. In the limit as the initial pulse width $2T$ approaches zero from above and/or as the propagation distance z tends to infinity these become the only, total, maxima of $X_U(\omega_r)$ along the real frequency axis. In the opposite limit, as the initial pulse width $2T$ tends to infinity and/or as the propagation distance z approaches zero from above, $X_U(\omega_r)$ exhibits a single total maximum located at the applied carrier frequency $\omega_r = \omega_c$ along the real frequency axis. When the applied carrier frequency is sufficiently above or below the (positive) resonance frequency of the gain medium, $X_U(\omega_r)$ exhibits a third local maximum along the positive real frequency axis; this occurs in the interval $0 < \omega_r < \omega_{\max}^+$ when ω_c is sufficiently below $\omega_{\max}^+$, while it occurs in the interval $\omega_r > \omega_{\max}^+$ when ω_c is sufficiently above $\omega_{\max}^+$. As the initial pulse width $2T$ increases and/or as the propagation distance z decreases, this becomes the dominant maximum of $X_U(\omega_r)$.

In addition, $X_U(\omega_r)$ may exhibit up to three local minima along the real frequency axis. One local minimum occurs in the frequency range $\omega_{\max}^- < \omega_r < \omega_{\max}^+$. When the applied carrier frequency is sufficiently above or below the (positive) resonance frequency of the gain medium, $X_U(\omega_r)$ may exhibit a second local minimum along the positive real frequency axis; this occurs in the interval $0 < \omega_r < \omega_{\max}^+$ when ω_c is sufficiently below $\omega_{\max}^+$, while it occurs in the interval $\omega_r > \omega_{\max}^+$ when ω_c is sufficiently above $\omega_{\max}^+$. As the initial pulse width $2T$ increases and/or as the propagation distance z decreases, the appearance of the second local minimum of $X_U(\omega_r)$ becomes increasingly likely. Conversely, as the initial pulse width $2T$ decreases and/or as the propagation distance z increases the appearance of the second local minimum is less likely. However, in the limit as the initial pulse width

$2T$ approaches zero from above and/or as the propagation distance z tends to infinity, $X_U(\omega_r)$ attains three minima at $+\infty$, 0, and $-\infty$ along the real frequency axis, since $X_G(\omega_r)$ lies completely along this axis in this limiting case.

This analysis leads to an approximate, heuristic evaluation of the unified integral expression (6) of the propagated field $A(z,t)$, when the contour of integration is taken to be the real frequency axis. In this case, this unified integral expression may be rewritten as

$$A(z,t) = \sum_k I_{Rk}(z,\theta') = \sum_k \left(\frac{1}{2\pi} \mathrm{Re}\left\{ i \int_{l_k}^{u_k} \tilde{U}_U \exp\left[\frac{z}{c} \Phi_U(\omega_r,\theta') \right] d\omega_r \right\} \right), \tag{C13}$$

where each of the integration intervals comprising the real frequency axis is suitably chosen to encompass a single one of the (up to three) local maxima ω_{mx_k}, $k \in N$ of $X_U(\omega_r)$. Therefore, for any given value of the input field and gain medium parameters as well as of the propagation distance (up to three of) the denoted terms $I_{Rk}(z,\theta')$, $k \in N$ appear in Eq. (C13), for any value of the space-time parameter θ'. From the preceding considerations concerning the behavior of $X_U(\omega_r)$, it is expected that the dominant contribution to the integral expression for $A(z,t)$ will arise from the spectral regions in the vicinity of the real frequencies ω_{mx_k}, $k \in N$ at which $X_U(\omega_r)$ attains its local maxima. It can be shown that when the relation

$$X_C(\omega_{mx_k}) < -X_G(\omega_{mx_k}) - \frac{1}{2} \frac{\partial^2 X_U(\omega_{mx_k})}{\partial \omega_r^2} (\omega_r - \omega_{mx_k})^2 \tag{C14}$$

is satisfied, the integral expression (C13) may approximately be evaluated by expanding each phase function appearing in the exponent of each of the terms $I_{Rk}(z,\theta')$, $k \in N$ in a Taylor series about the respective single real frequency ω_{mx_k} that lies in the corresponding integration interval, retaining only the first three terms in each such expansion [which is justified provided that the function $X_U(\omega_r)$ is sharply peaked about each of the frequencies where its local maxima occur] and subsequently performing the denoted integration. Upon performing this expansion, Eq. (C13) eventually yields

$$A(z,t) \cong \sum_k A_{Rk}(z,t) = \sum_k \left(\frac{1}{2\pi} \mathrm{Re}\left\{ i \tilde{U}_U \exp\left[\frac{z}{c} \Phi_U(\omega_{mx_k},\theta') \right] \times \left[\frac{\pi}{-\frac{1}{2} \frac{d^2 \Phi_U(\omega_{mx_k},\theta')}{d\omega_r^2}} \frac{c}{z} \right]^{1/2} \times \exp\left[\frac{\left[\frac{z}{c} \frac{\partial X_U(\omega_{mx_k},\theta')}{\partial \omega_r} \right]^2}{\frac{2z}{c} \frac{d^2 \Phi_U\left(\omega_{mx_k},\theta'\right)}{d\omega_r^2}} \right] \right\} \right), \tag{C15}$$

where $k \in N$. For the single resonance Lorentz-type dispersive and gain medium of interest, the inequality in Eq. (C14) appears to be satisfied at the local maxima points ω_{mx_k}, $k \in N$ of $X_U(\omega_r)$ for sufficiently broad input pulses and/or at sufficiently small propagation distances. In the ensuing, attention is restricted only to those cases where the inequality in Eq. (C14) is satisfied at the local maxima points ω_{mx_k}, $k \in N$; when this inequality is violated, one must resort to the unified asymptotic approach in order to obtain the complete uniformly valid description of the propagated field.

It follows from Eq. (C15) that the peak in the envelope of each of the terms $A_{Rk}(z,t)$ is approximately attained when $\partial Y_U(\omega_{mx_k},\theta')/\partial \omega_r = 0$, $k \in N$. Therefore, according to Eq. (C12), the peak in the envelope of each of the terms $A_{Rk}(z,t)$ approximately occurs at the respective space-time point

$$\theta_{\mathrm{peak}_{Rk}} = \frac{\partial}{\partial \omega_r} \left[\omega_{mx_k} n_r\left(\omega_{mx_k}\right) \right], \tag{C16}$$

so that each peak in the envelope approximately travels with the respective velocity

$$\upsilon_{\mathrm{peak}_{Rk}} = \frac{c}{\theta_{\mathrm{peak}_{Rk}}} = \left\{ \frac{\partial}{\partial \omega_r} \left[\frac{\omega_{mx_k} n_r\left(\omega_{mx_k}\right)}{c} \right] \right\}^{-1} = \upsilon_{\mathrm{group}}\left(\omega_{mx_k}\right), \tag{C17}$$

$k \in N$, which is equal to the classical group velocity at the real frequency where the respective local maximum of $X_U(\omega_r)$ occurs. Moreover, according to Eq. (C15), the respective frequency of oscillation associated with the peak in the envelope of each of the terms $A_{Rk}(z,t)$ is approximately given by

$$\omega_{\mathrm{peak}_{Rk}} = \omega_{mx_k} - \frac{\partial}{\partial \theta'} \left\{ \frac{\left[\frac{\partial Y_U(\omega_{mx_k},\theta')}{\partial \omega_r} \right]^2 \frac{\partial^2 Y_U(\omega_{mx_k},\theta')}{\partial \omega_r^2}}{2 \left| \frac{d^2 \Phi_U(\omega_{mx_k},\theta')}{d\omega_r^2} \right|^2} \right\}_{\theta' = \theta_{\mathrm{peak}_{Rk}}} \cong \omega_{mx_k}, \tag{C18}$$

$k \in N$. From Eq. (C15), the peak in the envelope of each term $A_{Rk}(z,t)$ is approximately given by

$$A_{\mathrm{peak}_{Rk}} = \frac{1}{2\pi} \mathrm{Re}\left\{ i \tilde{U}_U \exp\left[\frac{z}{c} \Phi_U\left(\omega_{mx_k},\theta_{\mathrm{peak}_{Rk}}\right) \right] \times \left[\frac{\pi}{-\frac{1}{2} \frac{d^2 \Phi_U(\omega_{mx_k},\theta_{\mathrm{peak}_{Rk}})}{d\omega_r^2}} \frac{c}{z} \right]^{1/2} \right\}, \quad k \in N. \tag{C19}$$

This approximate, heuristic analysis leads to the following description of the dynamical evolution of the propagated field: For a physically realizable input Gaussian-modulated harmonic wave having a very large initial pulse width $2T$ and/or at a very short propagation distance z in a single resonance Lorentz-type dispersive and gain medium, the local maximum of $X_U(\omega_r)$ that is located closer to the applied carrier frequency $\omega_c \geqslant 0$, i.e., the one that is located either at ω_{mx_1} or ω_{mx_2}, is the most dominant local maximum of $X_U(\omega_r)$ along the real frequency axis. Therefore, in the propagated field expression (C15), the dominant contribution to the propagated field arises either from the term $A_{R1}(z,t)$ or from the term $A_{R2}(z,t)$. Notice that for a physically realizable input Gaussian-modulated

harmonic wave with arbitrary, but nonvanishing, initial pulse width $2T$ and/or at an arbitrary, but finite, propagation distance z, the relation $X_U(\omega_{mx_3}) \ll X_U(\omega_{mx_1}), X_U(\omega_{mx_2})$ is always satisfied, so that the relation $A_{R3}(z,t) \ll A_{R1}(z,t), A_{R2}(z,t)$ is also always satisfied. Therefore, for an input Gaussian-modulated harmonic wave having a very large initial pulse width $2T$ and/or at a very short propagation distance z in the single resonance Lorentz-type dispersive and gain medium, the propagated field is compact in that its consists of a single Gaussian-shaped pulse component whose dynamical evolution is described by the corresponding term $A_{Rk}(z,t)$, $k = 1$ or 2. In particular, the oscillation frequency associated with the peak in the envelope of the propagated field is very close to ω_{mx_k} and, to a good approximation, this peak envelope occurs at the space-time point $\theta_{\text{peak}_{Rk}}$ that is given by Eq. (C16) so that it travels with the respective group velocity that is given by Eq. (C17). As the initial pulse width $2T$ is decreased and/or as the propagation distance z in the gain medium is increased, the real part of the unified phase function at its local maxima points ω_{mx_k}, $k \in N$ along the real frequency axis may violate the inequality in Eq. (C14) and the unified asymptotic approach must be invoked in order to obtain the complete uniformly valid description of the propagated field.

[1] P. B. Corkum and F. Krausz, Nature (London) **3**, 381 (2007)
[2] M. Hentschel, R. Kienberger, Ch. Spielmann, G. A. Reider, N. Milosevic, T. Brabec, P. Corkum, U. Heinzmann, M. Drescher, and F. Krausz, Nature (London) **414**, 509 (2001).
[3] A. Baltuška *et al.*, Nature (London) **421**, 611 (2003).
[4] E. Goulielmakis *et al.*, Science **305**, 1267 (2004).
[5] E. Goulielmakis *et al.*, Science **320**, 1614 (2008).
[6] E. Goulielmakis, V. S. Yakovlev, A. L. Cavalieri, M. Uiberacker, V. Pervak, A. Apolonski, R. Kienberger, U. Kleineberg, and F. Krausz, Science **317**, 769 (2007).
[7] A. Wirth *et al.*, Science **334**, 195 (2011).
[8] K. E. Oughstun, in *Electromagnetic and Optical Pulse Propagation 1: Spectral Representations in Temporally Dispersive Media*, Springer Series in Optical Sciences, Vol. 125 (Springer, New York, 2007).
[9] K. E. Oughstun, in *Electromagnetic and Optical Pulse Propagation 2: Temporal Pulse Dynamics in Dispersive, Attenuative Media*, Springer Series in Optical Sciences, Vol. 144 (Springer, New York, 2009).
[10] S. A. Akhmanov, V. A. Vysloukh, and A. S. Chirkin, *Optics of Femtosecond Laser Pulses* (American Institute of Physics, New York, 1992).
[11] G. P. Agrawal, *Nonlinear Fiber Optics* (Academic, San Diego, 2007).
[12] C. G. B. Garrett and D. E. McCumber, Phys. Rev. A **1**, 305 (1970).
[13] M. D. Crisp, Phys. Rev. A **1**, 1604 (1970).
[14] M. D. Crisp, Phys. Rev. A **4**, 2104 (1971).
[15] L. A. Vainshtein, Sov. Phys. Usp. **19**, 189 (1976).
[16] E. Varoquaux, G. A. Williams, and O. Avenel, Phys. Rev B **34**, 7617 (1986).
[17] I. P. Christov, IEEE J. Quantum Electron. **24**, 1548 (1988).
[18] R. Y. Chiao, Phys. Rev. A **48**, R34 (1993).
[19] A. Sommerfeld, Ann. Phys. **44**, 177 (1914).
[20] L. Brillouin, *Wave Propagation and Group Velocity* (Academic, New York, 1960).
[21] G. C. Sherman and K. E. Oughstun, Phys. Rev. Lett. **47**, 1451 (1981).
[22] K. E. Oughstun and H. Xiao, Phys. Rev. Lett. **78** 642 (1997).
[23] K. E. Oughstun, Comput. Sci. Eng. **5**, 22 (2003).
[24] P. Pleshko and I. Palocz, Phys. Rev. Lett. **22**, 1201 (1969).
[25] H. Jeong, A. M. C. Dawes, and D. J. Gauthier, Phys. Rev. Lett **96**, 143901 (2006).
[26] L. Casperson and A. Yariv, Phys. Rev. Lett. **26**, 293 (1971).
[27] S. Chu and S. Wong, Phys. Rev. Lett. **48**, 738 (1982).
[28] N. D. Hoc, I. M. Besieris, and M. E. Sockell, IEEE Trans. Antennas Propag. **33**, 1237 (1985).
[29] M. Tanaka, M. Fujiwara, and H. Ikegami, Phys. Rev. A **34**, 4851 (1986).
[30] C. M. Balictsis and K. E. Oughstun, Phys. Rev. E **47**, 3645 (1993).
[31] C. M. Balictsis and K. E. Oughstun, in *Ultra-Wideband, Short Pulse Electromagnetics 2*, edited by H. L. Bertoni, L. B. Felsen, and S. V. Pillai (Plenum, New York, 1995).
[32] K. E. Oughstun and C. M. Balictsis, Phys. Rev. Lett. **77**, 2210 (1996).
[33] C. M. Balictsis and K. E. Oughstun, Phys. Rev. E **55**, 1910 (1997).
[34] F. W. J. Olver, Stud. Appl. Math. Rev **12**, 228 (1970).
[35] R. A. Handelsman and N. Bleistein, Arch. Ration. Mech. Anal. **35**, 267 (1969).
[36] C. Chester, B. Friedman, and F. Ursell, Proc. Cambridge Philos. Soc. **53**, 599 (1957).
[37] T. Hosono, in *Proceedings of the 1980 International URSI Symposium on Electromagnetic Waves* (International Union of Radio Science, Munich, 1980).
[38] P. Wyns, D. P. Foty, and K. E. Oughstun, J. Opt. Soc. Am. A **6**, 1421 (1989).
[39] R. Safian, M. Mojahedi, and C. D. Sarris, Phys. Rev. E **75**, 066611 (2007).
[40] E. L. Bolda, J. C. Garrison, and R. Y. Chiao, Phys. Rev. A **49**, 2938 (1994).
[41] L. J. Wang, A. Kuzmich, and A. Dogariu, Nature (London) **406**, 277 (2000).
[42] S. Lang, *Complex Analysis* (Springer, New York, 1985).
[43] H. M. Nussenzveig, *Causality and Dispersion Relations* (Academic, New York, 1972).